Ph.D. Dissertation of Engineering

Spatial data collection methodology for estimating large-scale waste quantity based on Unmanned Aerial Systems and Terrestrial Laser Scanning

대형 폐기물량 산정을 위한 UAS와 TLS 기반

공간정보 구축기법 연구

August 2019

Graduate School of Seoul National University

Interdisciplinary Program in Landscape Architecture

Seungwoo Son

Spatial data collection methodology for estimating large-scale waste quantity based on Unmanned Aerial Systems and Terrestrial Laser Scanning

Advisor: Dong Kun Lee

A dissertation submitted in partial fulfillment of the requirements for the Degree of Doctor of Philosophy in Interdisciplinary Program in Landscape Architecture in Seoul National University

August 2019

Seungwoo Son

Approved by Thesis Committee

Chair Youngkeun Song (Seal)

Vice Chair Junguk Kang (Seal)

Examiner Jeongho Yoon (Seal)

Examiner Taehan Kim (Seal)

Examiner Dong Kun Lee (Seal)

Publications

Please note that some part of this dissertation proposal was written as stand-alone papers (see below), and therefore there is some repetition in the methods and results.

1. Son, S. W., Yoon, J. H., Jeon, H. J., Kim, D. W., & Yu, J. J. (2019). Optimal flight parameters for unmanned aerial vehicles collecting spatial information for estimating large-scale waste generation. *International Journal of Remote Sensing, 40*(20), 8010-8030.

Table of Contents

I. Introduction 1

II. Literature Review 7

1. Studies on Applying the UAS to Disaster Management 7

2. Accuracy of UAS-based 3D Model Construction 14

3. Disaster Waste Quantity 26

III. Materials and Methods 34

1. Optimal Flight Parameters for UAV Generating 3D Spatial Information 36

1.1. Design of UAV Flight 36

1.2. Photogrammetric Processing for the Acquisition of 3D Spatial Information 41

1.3. Assessment of the 3D Spatial Information Accuracy 43

1.4. Computation of the Amount of Waste 45

2. Comparison and Analysis of TLS and UAS Methodology for Optimal Volume Computation 47

2.1. TLS and UAS-based 3D Spatial Information Generation and Volume Computation 49

2.2. Comparison and Analysis of 3D Spatial Information 55

3. Multispace Fusion Methodology-based 3D Spatial Information Generating and Efficiency Analysis 57

3.1. Multispace Fusion Methodology-based 3D Spatial Information 57

3.2. Efficiency Analysis of 3D Spatial Information for Responding to Large-scale Disasters 58

III. Result and Discussion 59

1. Optimal Flight Parameters for UAV Generating 3D Spatial Information and Investigation of Feasibility 59

1.1. Generation of 3D Spatial Information using UAS 59

1.2. Assessment of the 3D Spatial Information Accuracy 64

1.3. Computation of the Amount of Waste and Optimal flights parameters 76

2. Comparison and Analysis of TLS and UAS-based 3D Spatial Information 84

2.1. Generation of 3D Spatial Information and Volume Computation using UAS 84

2.2. Spatial Comparison and Analysis 88

3. Multispace Fusion Methodology-based 3D Spatial Information Generating and Efficiency Analysis 93

3.1. Multispace Fusion Methodology-based 3D Spatial Information 93

3.2. 3D Spatial information Efficiency Analysis for Responding to Large-scale Disasters 96

IV. Conclusion 100

V. Bibliography 103

List of Figures

Figure 1 UAS utilization in disaster situations 9

Figure 2 Comparison and analysis of images before and after disasters using satellite images, UAS, etc 10

Figure 3 Examples of pixel intensity changes due to window movement ... 15

Figure 4 Process of SfM 18

Figure 5 Process of 3D point cloud generation based on UAV-MVS 19

Figure 6 Construction of DEM using UAS (left) and accuracy evaluation(right) 20

Figure 7 Construction of DEM and derivation of erosion amount by time series using UAS 22

Figure 8 Evaluation of 3D model height accuracy according to the number of GCPs 24

Figure 9 RMSE of digital aerial imagery orthophoto based on variation in flying altitude 25

Figure 10 Estimation sequence of disaster waste generation amount 30

Figure 11 Comparison of estimated and actual disaster waste generation amounts 31

Figure 12 Process workflow 34

Figure 13 Design of UAV flight and Scheme for cases 37

Figure 14 (a) Location of the study area and (b) Measuring points of ground control points 40
Figure 15 Measurement of CPs using VRS/RTK-GNSS: (a) Check poin ts, (b) Check points for Profile A-A' and (c) Check points for Pr ofile B-B' 44
Figure 16 Location of the study area (chapter 2 &3) 48
Figure 17 TLS scan positions and GCPs 50
Figure 18 GCP positions: (a) all GCPs; (b) GCPs placed without considering waste height; (c) GCPs placed considering waste height. 53
Figure 19 CP positions 54
Figure 20 DW variation of the target site for the UAV according to the altitude: (a) Takeoff point, (b) Above Ground Level and (c) Distance covered on the ground by on image in Width direction 60
Figure 21 (a) Case A with unregistered images and (b) case D showin g the overall registration of images 61
Figure 22 (a) RMSE with high levels overlap (FL : 80%- 90%, SL : 50%-60 %) and number of GCPs to flight altitude and (b) RMSE with the low levels (FL : 60%- 70%, SL : 30%- 40%) overlap a nd number of GCPs to flight altitude 67
Figure 23 RMSE with the same flight altitude and number of GCPs ac

cording to overlap : (a) Flight altitude 80 m, (b) Flight altitude 120m, (c) Flight altitude 150m 69
Figure 24 RMSE of each case according to the number of GCPs 70
Figure 25 Waste quantity computation process : (a) UAV flight, (b) Point Clouds, (c) DSM, and (d) Volume computation 76
Figure 26 Cross sections and cut and fill areas using UAV- and GNSS-based DEM 78
Figure 27 Point Clouds : (a) Case D-7 (High Accuracy), (b) Case G-1 (Low Accuracy) 79
Figure 28 DSM : (a) Case D-7 (High Accuracy), (b) Case G-1 (Low Accuracy) 80
Figure 29 TLS-based 3D spatial information (a) Point clouds, (b) DSM 84
Figure 30 UAS-based 3D spatial information: (a) Point clouds, (b) DSM .. 86
Figure 31 Side-view point clouds of the waste disposal site: (a)-1 TLS-based point cloud, (a)-2 UAS-based point cloud; (b)-1 TLS-based point cloud, (b)-2 UAS-based point cloud 90
Figure 32 Top view of the waste point cloud: (a)-1 TLS-based point cloud; (a)-2 UAV-based point cloud; (b)-1 TLS-based point cloud; (b)-2 UAV-based point cloud 91
Figure 33 Fusion method-based Point cloud: (a) Point clouds, (b) DSM 93

List of Tables

Table 1 Examples of UAV applications in disasters across the world 12

Table 2 Formula for estimating disaster waste generation amount 31

Table 3 Research materials 35

Table 4 GSD, UAV flight time, and number of images according to flight altitude and overlap 62

Table 5 Camera interior orientation parameters 63

Table 6 Statistical values of gimbal axes for each case 63

Table 7 Accuracy of x, y, z, and *xyz* locations in each case 64

Table 8 Value of each case parameters 66

Table 9 Time spent building 3D spatial information with the top 15 highest accuracy 81

Table 10 UAS-based point cloud accuracy depending on UAV flight cases 85

Table 11 Volume computation by UAV flight case 88

Table 12 Point cloud accuracy and volume computation results of the UAV, TLS, and TLS/UAV fusion models 94

Table 13 Time and accuracy of 3D spatial information construction Correlation analysis between variables 96

Table 14 Time requirements for TLS- and UAV-based point cloud generation 97

Table 15 Costs requirements for TLS-and UAS based point cloud generation 98

Abstract

Spatial data collection methodology for estimating large-scale waste quantity based on Unmanned Aerial Systems and Terrestrial Laser Scanning

Seungwoo Son
Interdisciplinary Doctoral Program in Landscape Architecture
Graduate School, Seoul National University
Supervised by Professor Dong Kun Lee

Damage to people, property, and the environment must be minimized through systematic and efficient handling of large-scale disasters throughout the entire process from prevention to the response stage. This study focused on the waste quantity calculations that are part of the response process during large-scale disasters. Studies on large-scale waste quantity calculations have been performed in the past, but actual measurements are difficult. Therefore, many studies are being performed on using information from previous instances to perform modeling and using technologies such as remote sensing to estimate waste quantities. This study calculated waste quantities based on UAS (unmanned aerial system), which is a technology that is often used these days. It evaluated the accuracy of this technology,

and it analyzed and compared the technology with existing technologies.

UAS can be seen as an overall process of using UAVs (Unmanned Aerial Vehicle) to capture images and analyzing them. Studies have been conducted in the past on using UAS to build 3D spatial information and evaluate accuracy, and they are being used integrally in a variety of fields. Similarly, 3D spatial information can be built using TLS (Terrestrial Laser Scanning), and these are chiefly used in the surveying field. This method's accuracy is excellent, and it is widely used in a variety of fields such as vegetation, construction, civil engineering, cultural assets, and topographical surveys. Large-scale waste can also be calculated by using TLS to build a 3D spatial information, but it is seen as unfeasible to use due to cost and time limitations.

This study is broadly divided into 3 parts. The first part is examining the feasibility of using UAS to build a 3D spatial information and calculate waste quantity. The process up to the point of using UAS to build a 3D spatial information was analyzed in detail, and optimal flight variables and other variables were found in order to examine the feasibility of calculating waste quantity. The second part is comparing and analyzing 3D spatial information based on TLS and UAS technology. The 3D spatial information were compared and analyzed using the M3C2 algorithm, and the optimal

waste quantity calculation methods were found. Finally, the third part is analyzing a combination of the 3D spatial information and the 3D spatial information' efficiency. The two technologies were combined to build a 3D spatial information, and their efficiency was analyzed to find the differences between the three methodologies (UAS, TLS, and the combined method), as well as find the optimal waste quantity calculation method.

The major flight variables are the flight altitude and image overlap. Another variable is the number of ground control points. In addition to this, the camera interior orientation and degree of gimbal shaking were analyzed. Through this study, the optimal variables among 56 cases were found. Unlike past studies, it was discovered that the results were contrary to previous studies due to the DW (Distance covered on the ground by on image in Width direction) in waste regions with a lot of altitude differences. Normally, as the altitude becomes lower, the accuracy of the 3D spatial information becomes higher, but in this study it was found that the accuracy became lower as the altitude became lower.

The accuracy of all 56 cases was analyzed, and it was found that there is a correlation between accuracy and the amount of waste. As the accuracy of the 3D spatial information increased, the calculated waste amounts became similar. Conversely, in 3D spatial information with low accuracy, it was

found that the waste amounts were different. Through this sequential process, the optimal UAS variables for calculating waste amounts were found, and it was possible to confirm the feasibility of calculating waste amounts based on 3D spatial information.

The M3C2 algorithm was used to compare the UAS and TLS-based 3D spatial information, and by doing so, it was possible to confirm the advantages and disadvantages of each model. As for accuracy, the RMSE of the UAS-based 3D spatial information was 0.032 m, and the RMSE of the TLS model was 0.202, making the UAS model's accuracy higher. The RMSE of the 3D spatial information which combined the two technologies was 0.030 m, and it showed the highest accuracy of the three methodologies. However, in terms of efficiency, the analyzed results were able to confirm that the UAS-based 3D spatial information had the optimal technology and methodology for large-scale waste amount calculations by creating a model which shows high accuracy in a short time. In addition, cost analysis results were able to confirm that the cost of building the UAS-based 3D spatial information was lower than that of TLS.

During large-scale disasters, it is necessary to respond in a relatively short time to minimize damage and perform a variety of decision-making. The UAS-based 3D spatial information building method found in this study

can be used for large-scale waste amount calculations and spatial decision-making.

Keywords: Spatial information, M3C2, Flight parameters, Computation of waste quantity

Student Number: 2014-30797

I. Introduction

The risk and severity of various types of disasters have risen due to phenomena such as abnormal climate change, complexity of social structures and urbanization, while disaster prediction and response are becoming increasingly difficult (Yoo, 2015; Son et al., 2016). Studies on disasters focus on not only the establishment of laws, institutions, and policies, but also on diverse aspects that are concerned with pre-disaster mitigation and prevention step and preparedness and planning step, and post-disaster response and recovery steps, as categorized based on the time of a disaster event (McLoughlin, 1985; Petak, 1985).

In particular, when a large-scale disaster occurs, it inflicts severe damages to human life, economy and culture as well as to the environment. The waste generated by a disaster not only affects the disaster response and recovery activities but also poses a grave threat to the environment and public health (Brown et al., 2011). The research and interest on disaster response, which involves damage analysis and waste treatment upon a disaster event, have continuously increased, and a large volume of disaster waste may have a negative influence on the land and surrounding environment of the affected area as well as on drinking water when the

leachate flows into the ground water; hence, the waste generated by a disaster can lead to complex environmental pollution. The magnitude of the environmental impact from disaster waste has not been quantitatively studied although a number of studies focused on the quantification of the risks entailed by disaster waste (Hu and Sheu, 2013). The interest on the potential influence of disaster waste on the environment, in particular, has continued to grow (Dijkstra et al., 2002). Disaster waste is intricately related to the environment, and it has brought adverse effects on both the physical aspect of pollution and the management of the environment (Brown et al., 2011).

The potential environmental impact of disaster waste may be influenced by the specific type of waste generated by different disaster situations and the duration before treatment, in addition to the complex interaction with the surrounding environment. A toxic substance may arise from disaster waste to have an effect on the surrounding environment and human. Other potential and complex negative influence may be imparted on the environment such as drinking water, agriculture, ecosystem and soil, upon the release of pollutants to the air and the river (Srinivas and Nakagawa, 2008). Thus, it is essential that disaster response and recovery must be based on rapid and accurate analysis of waste generated by a disaster event.

In Korea and overseas, guidelines and manuals on disaster response measures and waste treatment have been developed and implemented according to the situations. The U.S. Federal Emergency Management Agency (FEMA) and Environmental Protection Agency (EPA) provide guidelines on disaster response and waste treatment upon a disaster event, which suggest appropriate capacity and location of the temporary storage sites for disaster waste. Japan and Australia also provide guidelines regarding selection criteria, location and capacity of temporary storage sites. Nonetheless, for rapid transportation and treatment of disaster waste prior to its translocation to a temporary storage site, it is necessary to first analyze the quantity of waste generated by a disaster to allow accurate decision-making on waste treatment, but in practice, it is difficult to quantify a large volume of disaster waste.

Geographic Information System (GIS) was used in the U.S. for developing The Hazards U.S. Multi-Hazard (HAZUS-MH) model in order to predict the type and quantity of disaster waste generated by flood, hurricane and earthquake, while simulations were run to predict the physical, social and economic damages as well as damages to social infrastructures (Jo et al., 2016). In addition, satellite images and GIS were used in Japan to acquire the information on disaster damage, analyze flooded areas and

bathymetric distributions, and estimate the disaster waste quantity (Asari et al., 2013). However, appropriate use of satellite images or aerial images in the right time of need is difficult in practice. Disaster waste quantities were predicted in Taiwan based on past flood disaster cases and using population density, flood damage area and precipitation as variables (Chen et al., 2007). In Australia, disaster waste quantities were estimated based on the buildings in the affected area and their dimensions by devising a case of waste quantity for each disaster type (Jo et al., 2016).

In Korea, the most frequent disasters mainly include landslide and waterlogging in urban areas due to flood, and response measures have been developed accordingly. The Ministry of Environment makes the prediction on disaster waste quantity in consideration of the past ten-year data of the flood-generated waste quantity, expected level of flooding, and number of houses, and when sufficient data of flood damage is unavailable, it recommends the use of unit waste generation per flooded building (Jo et al., 2016). As can be seen, past cases or modelling are used to predict the information regarding the damage and generated waste quantity for disaster response and recovery. In Korea and overseas, most estimations for disaster response or disaster waste quantity prediction are based on satellite images or unit waste generation; however, problems regarding utility and accuracy

have consistently been raised. Thus, it is necessary to carry out rapid and accurate analysis of the current state and waste estimation following a disaster event.

The level of disaster damage and disaster waste quantity vary according to the scale of disaster and circumstances in the affected area. Looking into the actual disaster cases that occurred in certain regions in the U.S. showed that the quantity of disaster waste generated by a single disaster event was 5 - 15 times greater than the annual regional waste (Reinhart and Mccreanor, 1999). As such, it is difficult to determine the level of disaster damage and the quantity of a large volume of disaster waste so that studies and policy-making are being carried out globally for information construction on disaster damage using satellite images or waste quantity prediction on unit waste generation.

Debris or large-scale waste caused by disasters can take many forms. There are many different methods to manage and dispose depending on the type of waste, but waste quantity is estimated beforehand, so it is moved to temporary waste transfer station regardless of its type for prompt management and disposal. In other words, waste quantity is solid waste that can be estimated.

This study thus developed an Unmanned Aerial System (UAS)-based 3D

spatial information and a 3D spatial information using multi-space convergence technique among the response measures prepared for post-disaster rather than pre-disaster use, with an ultimate goal to produce a disaster map and estimate disaster waste quantity while analyzing their accuracy.

II. Literature Review

1. Studies on Applying the UAS to Disaster Management

UAS is widely used in diverse fields in Korea and overseas. It is also actively applied in studies focusing on landscape architecture, forestry, agriculture, coast, topography, and environmental planning. UAS is generally called Drone or Unmanned Aerial Vehicle (UAV). The term Drone in the past was mainly used under military context and now it is commonly used by the media and general public. The term UAV is mainly used to indicate the unmanned aircraft itself (Son et al., 2016). On the other hand, UAS indicates a system that explores the spatiotemporal information of the subject in the image and sets it into 3D realization through the computer vision that interprets the images received from the Global Navigation Satellite System (GNSS), Inertial Navigation System (INS), Charge Coupled Device (CCD) or Complementary Metal-Oxide Semiconductor (CMOS), or the laser scanning technology loaded on the UAV (Lee, 2015; Yoo et al., 2016). In other words, it can be seen as the overall process of acquiring UAV images and using them in post-treatment.

The need for UAS in disaster management has been consistently emphasized as it entails considerably wide scope of application. With continuing increase in the use of UAS in actual disaster situations, the technology has undergone rapid advancement. Studies on applying the UAS to disaster management takes different approaches such as one based on the time of disaster; i.e. before, after, in the middle of a disaster event, or one that involves technical standpoints on UAS. Erdelj and Natalizio (2016) analyzed previous studies on UAS under the perspectives of disaster management. Each previous study reports on the application of UAS or wireless sensor network technology and the key disaster response measures based on UAS. The domains where UAS was applied in a disaster situation were the following six: i) early warning systems; ii) disaster information fusion; iii) situational awareness; iv) damage assessment; v) standalone communication system; vi) search and rescue missions. As such, while the studies on applying the UAS to disaster situations are ongoing, it can be seen that the scope of study is considerably broad. Depending on the scale or time of a disaster event, various studies were carried out, mostly focusing on a large-scale disaster situation and post-disaster investigation. This is thought to be due to an advantage of UAS where it is possible to apply extensive spatial monitoring technology.

In the past, most studies used satellite images and aerial photos to estimate and assess the level of damage following a disaster event, based on which plans were established for preparedness and recovery while decisions were made regarding damage compensation.

Related works		Disaster stages			Technology		UAV-assisted applications					
Authors	Year	Pre-disaster preparedness	Disaster assessment	Post-disaster response & recovery	WSN	UAV	Monitoring, forecast, EWS	Information fusion	Situational awareness	Damage assessment	Standalone comm. system	SAR missions
Frigerio et al [11]	2014	•			•		•					
Ueyama et al [30]	2014	•		•	•	•	•				•	
Erman et al [8]	2008	•	•		•	•	•		•			
Chen et al [5]	2013	•	•		•		•	•				
Bartoli et al [3]	2015	•	•		•			•				
Kumar et al [16]	2004		•		•	•		•		•		
Mosterman et al [20]	2014		•		•	•		•				
Sardouk et al [27]	2010		•	•	•			•				•
Grocholsky et al [14]	2006		•			•			•			
George et al [13]	2010		•		•				•			
Pogkas et al [25]	2007		•	•	•				•			•
Murphy et al [21]	2008		•	•		•			•			•
Wada et al [31]	2013		•			•				•		
Ezequiel et al [9]	2014		•			•				•		
Kruijff et al [15]	2012		•	•		•				•		•
Fujiwara and Watanabe [12]	2005			•	•						•	
Bai et al [2]	2010			•	•						•	
Fragkiadakis et al [10]	2011			•	•						•	
Nelson et al [22]	2011			•		•					•	
Tuna et al [29]	2012			•	•	•					•	
Morgenthaler et al [19]	2012			•		•					•	
Dalmasso et al [6]	2012			•		•					•	
Marinho et al [17]	2013			•		•					•	
Minh et al [18]	2014			•	•						•	
Carli et al [4]	2014			•	•						•	
Di Felice et al [7]	2014			•		•					•	
Robinson and Lauf [26]	2013			•		•					•	•
Nourbakhsh et al [23]	2005			•	•							•
Tuna et al [28]	2014			•	•	•						•

Figure 1 UAS utilization in disaster situations (Erdelj and Natalizio, 2016)

Nonetheless, the use of satellite images or aerial images is often limited to a great extent in terms of required time or situation. Thus, studies were carried out recently to precisely analyze the damages inflicted by a disaster,

based on UAS images and satellite images (Kakooei and Baleghi, 2017). In general, they obtained pre-disaster information of satellite images then photographed post-disaster images by applying the UAV in order to comparatively analyze the two images for by applying the UAV in order to comparatively analyze the two images for estimating the level of damage.

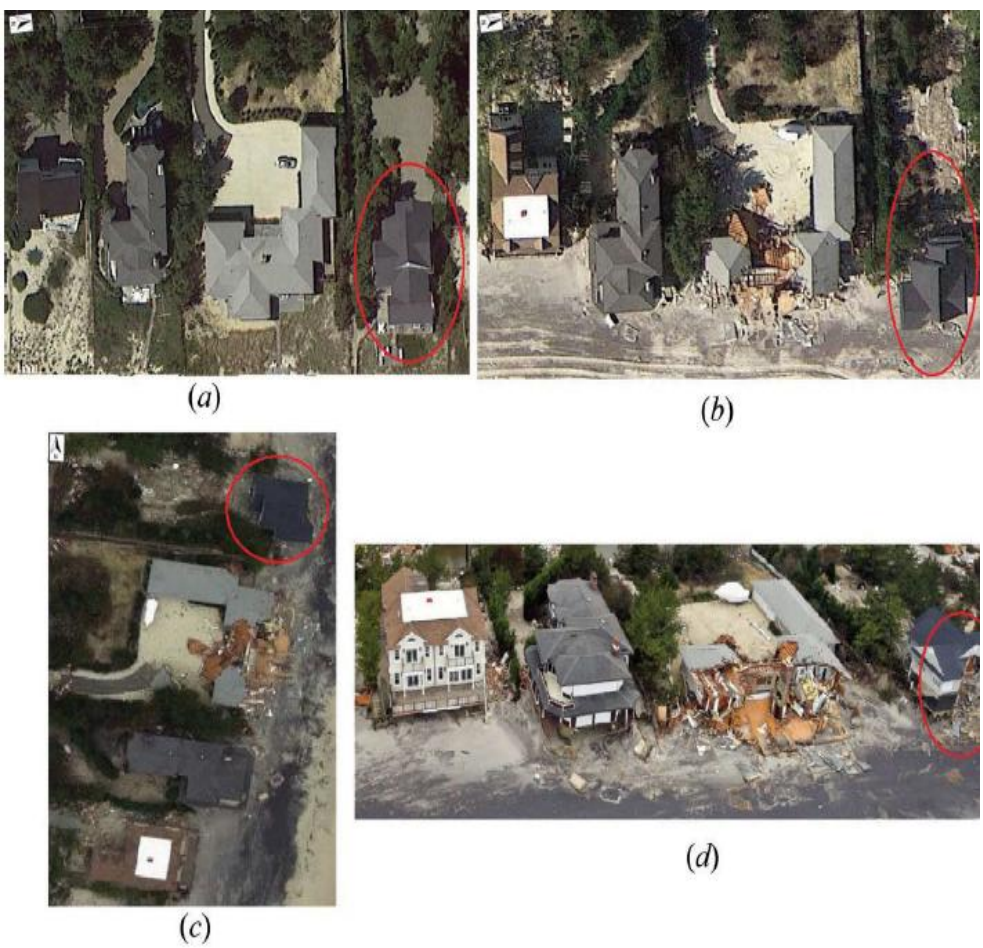

Figure 2 Comparison and analysis of images before and after disasters using satellite images, UAS, etc (Kakooei and Baleghi, 2017)

As such, the post-disaster images of the affected area enabled relatively fast and precise analysis of damages (Ezequiel et al., 2014) or a 3D model of the affected area was constructed to precisely estimate the level of damage (Meyer et al., 2015). Furthermore, studies were carried out on the ways to apply the UAS to different disaster situations including forest fire, earthquake, and flood (Restas, 2015).

The UAV-assisted cases of global large-scale disaster situations show that different UAV is applied according to the goals of each disaster response. Through this, it can be seen that the use of UAV is categorized into search, tracing and mapping, structural inspection, and debris estimation, and that UAV is applied mostly to search and mapping.

For a large-scale disaster, UAS brings in the necessary technology within a short time and covers a vast range of space. Studies mainly focus on analyzing the level of post-disaster damage to complement the limitation of conventional satellite or aerial images. In an actual case of a large-scale disaster, UAS was applied during the steps such as mapping and debris estimation, and despite its importance being discussed, the current approach still remains at a technical level.

A disaster map produced based on UAS enables crucial decision-making such as those for disaster response and recovery, implying the need to

overcome the limitation of using the conventional satellite or aerial images. Furthermore, the current study and technology regarding disaster waste estimation are less than sufficient and applying the UAS seems to require a solid foundation laid by continued research on its accuracy and precision.

Table 1 Examples of UAV applications in disasters across the world

Classification		UAV classification			Application			
Year	**Disaster**	**UAV**	**Fixed Wing**	**Rotary**	**Search**	**Reconaissance and mapping**	**Structural Inspection**	**Estimation of debris**
2005	Hurricane Katrina Response (USA)	AeroVironment Raven	∨		∨	∨		
		Evolution	∨		∨	∨		
		iSENSYST-Rex		∨	∨	∨		
		Silver Fox	∨		∨	∨		
2005	Hurricane Katrina Recovery (USA)	iSENSYS IP3		∨			∨	
2005	Hurricane Wilma (USA)	iSENSYS T-Rex		∨		∨	∨	
2007	Berkman Plaza Ⅱ	iSENSYS IP3		∨			∨	
2007	L'aquila Earthquake (Italy)	Custom		∨		∨	∨	
2009	Typhoon Morakot (Taiwan)	unknown		∨		∨		
2010	Haiti Earthquake (Haiti)	Elbit Skylark	∨			∨		
2011	Christchurch Earthquake (NZ)	Parrot AR.Drone		∨			∨	

2011	Tohoku Earthquake (Japan)	Pelican					∨	
2011	Fukushima Nuclear Emergemcy (Japan)	Custom	∨			∨		
		Honeywell T-Hawk		∨		∨	∨	
2011	Evangelos Florakis Naval Base Explosion (Cyprus)	AscTec Falcon		∨		∨	∨	
		AscTec Hummingbird		∨		∨	∨	
2011	Thailand Floods (Thailand)	FIBO UAV-1	∨			∨		
		FIBO UAV Glider	∨			∨		
		SIAM UAV	∨			∨		
2012	Finale Emilia Earthquake (Italy)	NIFTi 1		∨			∨	
		NIFTi 1		∨			∨	
2013	Typhoon Haiyan (Philippines)	unknown	∨			∨		
2013	Lushan China Earthquake	HW18 (Ewatt Hover Wings)	∨	∨	∨	∨		
2013	Boulder Colorado floods (USA)	Falcon Fixed	∨			∨		
2014	SR530 Mudslides Response (USA)	DJI Phantom		∨		∨		
		AirRobot 100						
		Insitu ScanEagle	∨					
		Precision Hawk	∨			∨		
2014	SR530 Mudslides Recovery (USA)	AirRobot 180		∨				∨
		Precision Hawk	∨					∨
2014	Balkans flooding	ICARUS		∨		∨		∨

	(Serbia, Bosnia-Herzegovina)	custom						
2014	Collbran Landslide (USA)	Falcon Fixed	∨		∨	∨		
		Falcon Hover		∨	∨	∨		
2014	Yunnan China Earthquake (China)	Parrot AR Type 2		∨		∨		
2015	Bennett Landfill SC (USA)	PrecisionHawk	∨					∨

Modified from American Red Cross (2015)

2. Accuracy of UAS-based 3D Model Construction

The study and technology for UAS-based 3D model construction show a trend of rapid increase. 3D models are widely used in various fields including environment, architecture, civil engineering, and topography. In the past, 3D models were constructed using satellite or aerial images, but recent studies have consistently focused on the efficiency and accuracy of UAS-based 3D models.

In the photo measurements based on UAS, the Scale Invariant Feature Transform (SIFT) and Structure from Motion (SfM) algorithms are used to automatically align the images and form the data of point groups with 3D coordinates, to construct a 3D model. The 3D model is given geometric correction through automatic aerotriangulation in consideration of GCP (Seibert and Teizer, 2014).

SIFT allows the matching of multiple images in terms of scale, rotation, and illumination (Lowe, 2004). For a large number of images taken by UAV, it is necessary to detect the main features and have them matched. The features should be easily distinguished and locate an identical point in space even in the images varying in angle and illumination. These features are often found in a building or corners of a parking line or a crossroad, and the usual way to find a feature can be described through Harris corner detection algorithm. Looking at Figure 3, the changes in the window while moving it can be observed. When moving the window, the flat areas throughout the window do not display any changes in pixel intensity, and for the edges, no change in pixel intensity is shown along the direction of the edge. But for the corners, distinctive changes in pixel intensity can be seen along all directions.

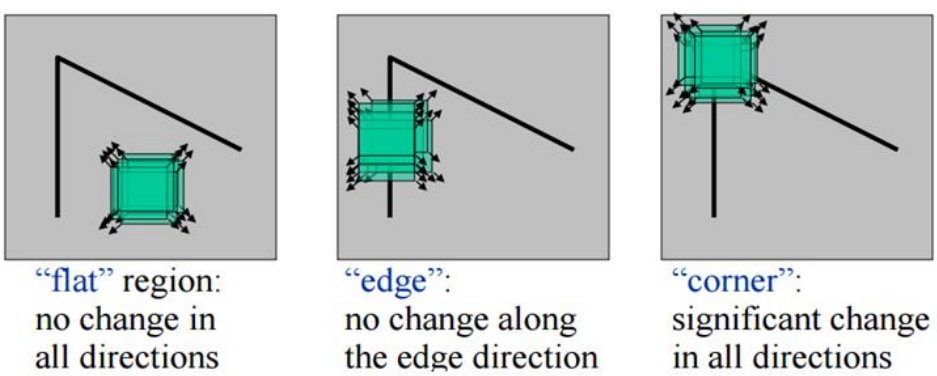

Figure 3 Examples of pixel intensity changes due to window movement (Frolova and Simakov, 2004)

The pixel intensity within the window, and the degree of changes in pixel intensity upon moving the window, are represented by the equation below:

$$E(u,v) = \sum_{x,y} w(x,y)[I(x+u, v+v) - I(x,y)]^2 \quad \text{(Eq. 1)}$$

E(u, v) = Change in pixel intensity (Change in the image)

w(x, y) = x, y coordinates within the window

I = Intensity

For flat areas, a value close to 0 would be produced as almost no change is shown by the intensity, but for areas with many corners, the large change in intensity would lead to a large value. Therefore, to detect corners, it is required to find the points where the largest changes in pixel intensity occur. Assuming that the changes in the window are very small and using the gradient (Lee et al., 2016) to apply the Taylor series, the following equation results:

$$E(u,v) \approx [u,v] M \begin{bmatrix} u \\ v \end{bmatrix} \quad \text{(Eq. 2)}$$

E(u, v) = Change in pixel intensity (Change in the image)

M = Matrix

When two eigenvalues of 2×2 matrix M are λ1 and λ2 (λ1 ≥ λ2), the E representing the change in the image reaches its maximum value if the window is moved along the direction of the eigenvector of λ1, and if it is moved along that of λ2, the E reaches its minimum value (Lee et al., 2016). Therefore, by calculating two eigenvalues of M, whether a given area is flat or a corner can be determined. In other words, when both values are large, it is a corner; when both are small, it is a flat area; when one is large but one is small, it is an edge. As shown, most algorithms in the past used to extract the features of an image based on Harris corner detection. In SIFT, unlike Harris algorithm for detecting corners, the value of Laplacian function is used (Lee et al., 2016) where a sequence of steps additionally take into account the changes in image brightness and scale space, and localization is given to the features, while the finally selected features are used to estimate the orientation. Through this process based on various algorithms, features are detected and images are matched.

Recently, UAS technology was coupled to SfM algorithm (Westoby et al.,

2012; Fonstad et al., 2013; Dietrich, 2016; Smith et al., 2016; Vazquez-Tarrio et al., 2017) to construct Digital Elevation Model (DEM) or Digital Surface Model (DSM) accurately and within a relatively short period of time. This can be attributed to the 2D images taken by UAV allowing the estimation of 3D points. Through the use of features detected by the previously discussed SIFT, the images are matched, and based on Epipolar Geometry estimation, the relative positions are deduced.

Figure 4 presents the SfM procedure that is mainly used in studies on computer vision technology, and motions can be estimated through visual tracking to produce a 3D map (Yilmaz and Karakus, 2016).

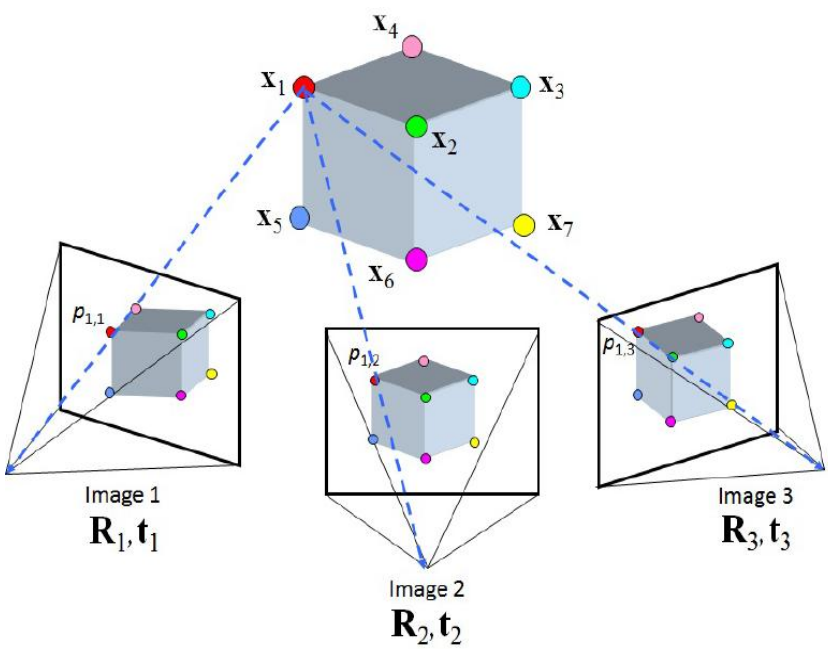

Figure 4 Process of SfM (Yilmaz and Karakus, 2016)

From the 2D images taken of a specific target from various angles and locations, features are detected and matched with those of the adjacent images. Based on the matched features and using Epipolar Geometry representing the geometric relation between the two images, the relative position and direction between the two cameras are estimated and from these, the 3D positions of the features are traced back (Lee et al., 2016).

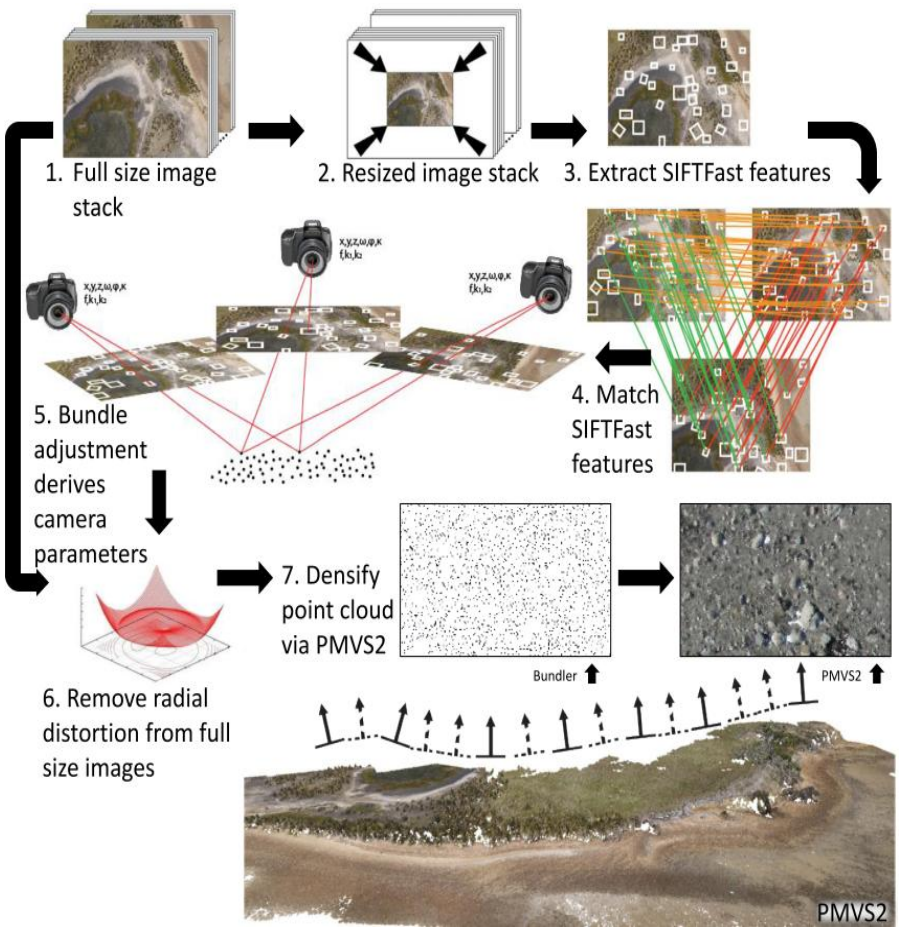

Figure 5 Process of 3D point cloud generation based on UAV-MVS (Harwin and Lucieer, 2012)

Most studies on UAS-based 3D models construct DEM, DSM, or Digital Terrain Model (DTM) as the most representative models in 3D, after which the model is applied in practice or its accuracy is tested. Uysal et al. (2015) applied UAS to the construction of DEM and evaluated its accuracy (Fig. 6). Ground Control Point (GCP) was measured for the target area and compared with the constructed DEM. In analysis result of the accuracy, the difference from the actual topography was approximately 6 cm, implying a comparatively high accuracy. In addition, studies have applied UAS to the construction of DSM for waterfront or coast areas and compared it with the DSM obtained from LiDAR for accuracy evaluation (Mancini et al., 2013; Lee et al., 2015).

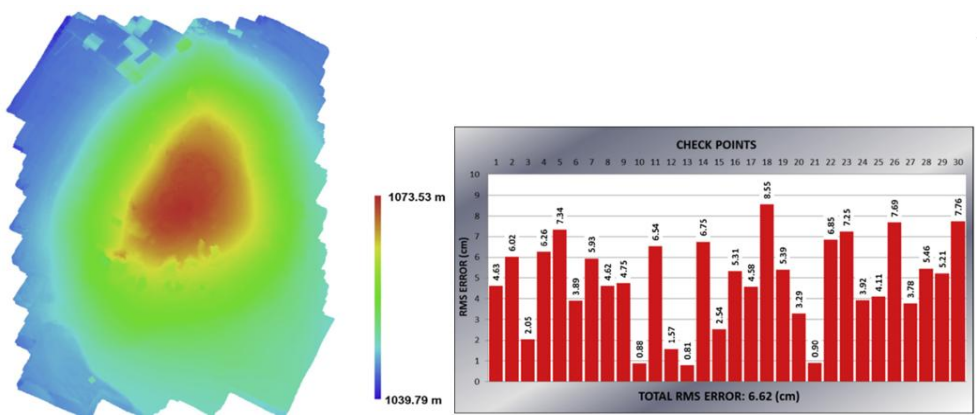

Figure 6 Construction of DEM using UAS (left) and accuracy evaluation (right) (Uysal et al., 2015)

Studies are continuing to apply the UAS to the construction of DEM or DSM and verify the accuracy; however, recent studies are focusing on environment or topography monitoring, surveys, and vegetation structure analysis, based on the accuracy of UAS. To verify the accuracy of UAS-based 3D model, the GCP of the study area is measured and the accuracy is evaluated based on the RMSE value. RMSE is utilized to assess model accuracy in recent studies. Giannetti et al.(2018) compared point clouds using techniques of ALS, UAV and others to predict forest growing stock volume. R^2, mean difference, and RMSE were used in comparison and assessment. Gonçalves and Henriques (2015) performed a monitoring study using UAV filming techniques and assessed location accuracy of DSM using RMSE. Kalacska et al. (2017) focused on wetland to construct 3D point clouds using UAV, GPS and others, also performed comparison and assessment of 3D point clouds using R^2 and RMSE.

Pineux et al. (2017) constructed the DEM for agricultural watershed using the UAS during the period between 2011 and 2014, then quantitatively deduced the erosion according to time series (Fig. 7).

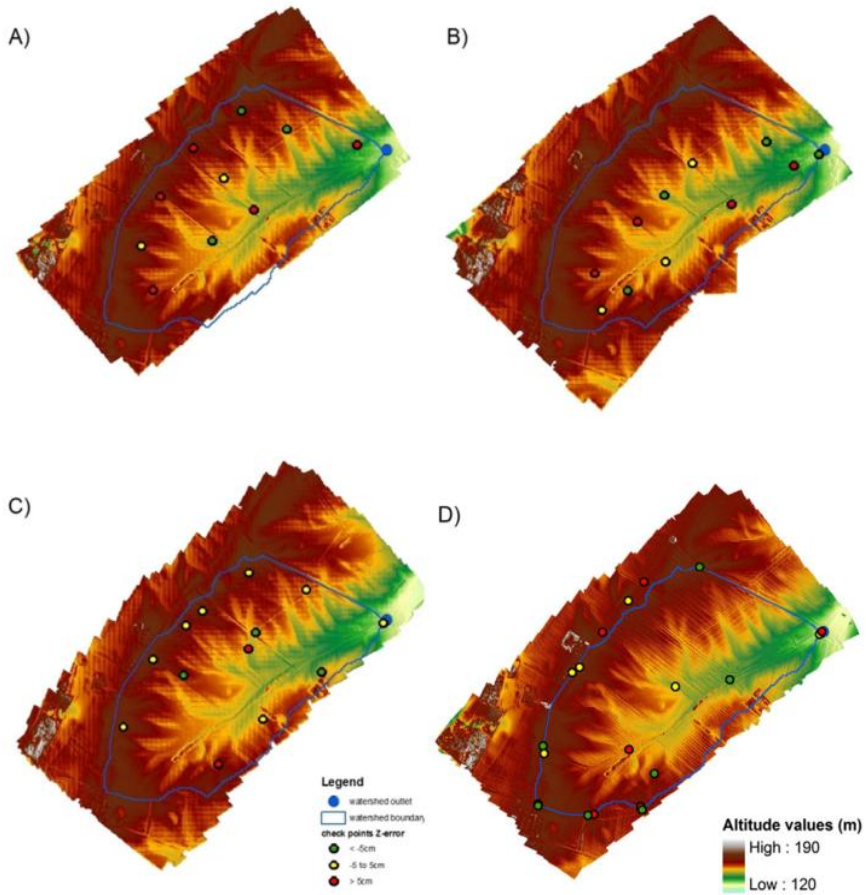

Figure 7 Construction of DEM and derivation of erosion amount by time series using UAS (Pineux et al., 2017)

The study area was not relatively large but posed a few challenges to the direct measurement and monitoring. The study can be viewed as one that solved such limitations through the use of UAS. As such, on the premise of high accuracy, the application of UAS has recently extended to diverse fields regarding the environment. Coveney and Roberts (2017) used the

UAS to construct the DEM for a flood prediction model, and evaluated the accuracy of the DEM using Root Mean Square Error (RMSE) in consideration of variables such as GCP. Likewise, modelling studies have continued since the past in the fields such as biodiversity distribution, flood, landslide, and climate change. Despite the strong emphasis on modelling studies that solve problems and prepare measures in the field of concern by predicting the future, discussions on uncertainty have steadily been pursued.

Different test methods have been proposed to overcome the uncertainty but what is most important is the applied data. The data constructed using UAS have shown high resolution and accuracy compared to the data constructed using satellite or aerial images, and the credibility of the modelling studies based on such data is likely to improve by a few degrees.

The point clouds constructed using UAS are under the influence of flight variables, and Agüera-Vega et al. (2017) tested the accuracy of 3D models with respect to the number of GCP, which led to the finding that installation of 15 or more GCP is required for relatively high accuracy of 3D models (Fig. 8).

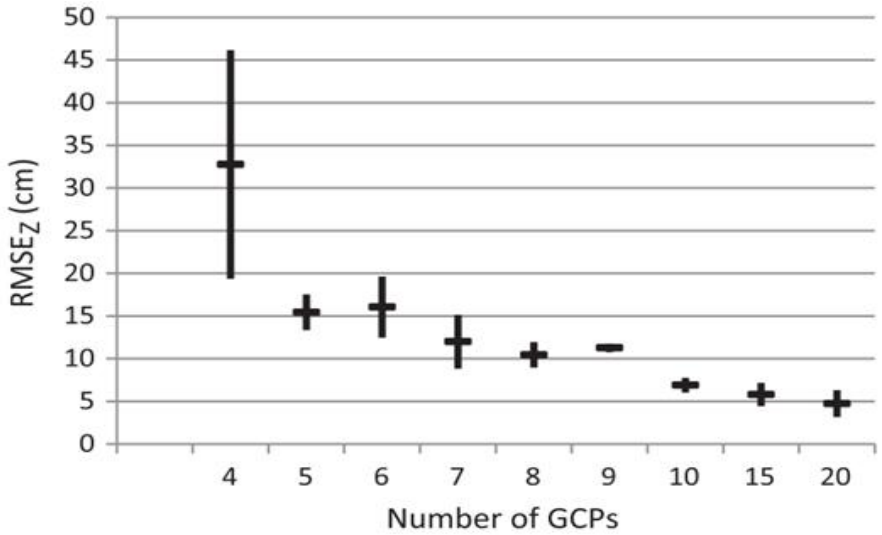

Figure 8 Evaluation of 3D model height accuracy according to the number of GCPs (Agüera-Vaga et al., 2017)

Among the flight variables such as GCP, the flight altitude is a critical factor that directly affects the accuracy of 3D models as well as the ground sample distance. Mesas-Carrascosa et al. (2016) highlights flight altitude as the most important flight variable, and Udin and Ahmad (2014) evaluated the accuracy of the X(m), Y(m), Z(m) of 3D models by setting the flight altitude at a range between 40 m and 100 m (Fig. 9). Studies have also analyzed the accuracy by varying the flight variables such as flight altitude and redundancy and whether GCP is being used (Mesas-Carrascosa et al., 2016).

Flying altitude	Aerial Triangulation	RMSE (m)			
		X(m)	Y(m)	Z(m)	MEAN (m)
40m	10 check points	±0.411	±0.156	±0.178	**±0.249**
60m	10 check points	±0.415	±0.159	±0.212	**±0.262**
80m	10 check points	±0.410	±0.163	±0.287	**±0.287**
100m	10 check points	±0.415	±0.149	±0.324	**±0.296**

Figure 9 RMSE of digital aerial imagery orthophoto based on variation in flying altitude (Udin and Ahmad, 2016)

In the past, 3D models such as ground elevation model were constructed using satellite or aerial images to be applied in various fields. Recently, however, most studies focus on the UAS-based 3D model construction. Initially, the studies on UAS-based 3D models measured the GCP of actual target areas and analyzed the accuracy; nevertheless, the importance of flight variables in constructing 3D models have attained growing attention recently. When only a number of set variables are considered without comprehensively reflecting the flight variables, inconsistent results were obtained among the studies. For instance, Uysal et al. (2015) and Agüera-Vega et al. (2017) showed similar values of vertical accuracy for images taken at the altitudes of 60 m and 120 m, respectively. Mesas-Carrascosa et al. (2016) had their images taken in complex consideration of the flight

altitude, imaging redundancy, and use of GCP, but still faced insufficient consideration of the number and location as well as altitude above a certain height in regard to GCP, which have persistently been pointed out.

The target areas for UAS-based 3D model construction often show fluctuating topography or large differences in elevation. For disaster-affected areas, the differences in elevation or shape of the surface are thought to vary according to destruction of buildings or damaged trees. Thus, only with complex and detailed consideration of flight variables, would accurate disaster maps be produced and disaster waste quantity be estimated.

3. Disaster Waste Quantity

The quantity of disaster waste vary according to the type and scale of disaster and the circumstances in the affected area. Disasters occur in different forms: natural disasters such as flood, hurricane, earthquake, and landslide; man-made disasters such as explosion and destruction, all of which equally generate disaster waste due to the destruction of buildings or facilities and landslide. In Korea, disaster wastes are mostly generated from hurricane or flood. Thus, the cases of predictive estimation of flood-generated waste quantity were the focus of analysis and investigation.

The U.S. Army Corps of Engineers developed an equation for estimating disaster waste quantity (EPA, 2008) that is currently being used by the EPA in the U.S. The equation is as described below:

$$Q = H \times C \times V \times B \times S \quad \text{(Eq. 3)}$$

Q = Expected quantity of waste
H = Number of households or people
C = Category of hurricane
V = Vegetation density
B = Percentage of business structures
S = Standardized precipitation index

Using hurricane category, population size, vegetation density, percentage of business structures, and standardized precipitation index, the equation is applied to estimating the expected quantity of waste upon an actual disaster event, to provide supporting evidence for the policy making.

The FEMA gives The Hazards U.S. Multi-Hazard (HAZUS- MH) model based on GIS (FEMA, 2007; Jo et al., 2016) and the equation is as described below:

$$CY = L' \times W' \times S \times 0.20 \times VCM \quad \text{(Eq. 4)}$$

CY = Disaster waste quantity within a cubic yard (0.765 m^3)
L = Length of building
W = Width of building
S = Height of building from the exposed floor
VCM = Vegetation cover multiplier

HAZUS-MH model gives an equation that estimates the quantity of disaster waste within a cubic yard (0.765 m^3) using building length and width and vegetation cover multiplier. It is used for decision-making regarding response and policy upon an actual disaster event.

In Japan, waste quantity is estimated based on unit waste generation. For flood damage, the unit waste generation per flooding depth and that per level of damage on houses were applied to two separate equations: ENV1 and ENV2 for waste quantity estimation according to the level of damage, or depending on the local government, an independent equation was developed and used for the estimation (Kim et al., 2012; Jo et al., 2016). The equations ENV1 and ENV2 for disaster waste quantity estimation are as shown below:

ENV1. $Y = 3.79x_1 + 0.08x_2$ (Eq. 5)

Y = Disaster waste quantity

x_1 = Number of houses flooded above floor

x_2 = Number of houses flooded below floor

ENV 2. $Y = 16.1x_1 + 1.2x_2 + 1.37x_3 - 0.015x_4$ (Eq. 6)

Y = Disaster waste quantity

x_1 = Number of houses flooded above floor: 0 - 49 cm

x_2 = Number of houses flooded above floor: 50 - 99 cm

x_3 = Number of houses flooded above floor: 100 cm -

x_4 = Number of houses flooded below floor

In addition, in Annakashi prefecture in Japan, the equation for estimating the quantity of waste generated by building destruction is applied after subdividing the variables into the total floor area of damaged building and the weight of debris per area. Figure 10 presents the 2014 Guidelines on Disaster Waste Response Measures of the Ministry of Environment in Japan, developed a method of estimating the disaster waste quantity due to flood damage and earthquake by differentiating the time before and after the disaster (Jo et al., 2016). Before the disaster, waste quantity is estimated using unit waste generation according to the regional disaster prevention plans and in reference to past cases. After the disaster, information on disaster damage such as satellite or aerial images is used to analyze the number of affected buildings and households, then using unit waste

generation, more elaborate estimation of the waste quantity is carried out. As shown, satellite images or GIS are used in analyzing the level of damage and estimating the disaster waste quantity (Asari et al., 2013).

Disaster waste quantity varies according to the current state of affected area, population, the type of disaster and duration of the disaster event. In Taiwan, parameters that influence waste generation were deduced, and based on this, an equation for estimating waste quantity was developed (Chen et al., 2007). The parameters influencing waste generation included the building type, flood damage area, precipitation duration, and population

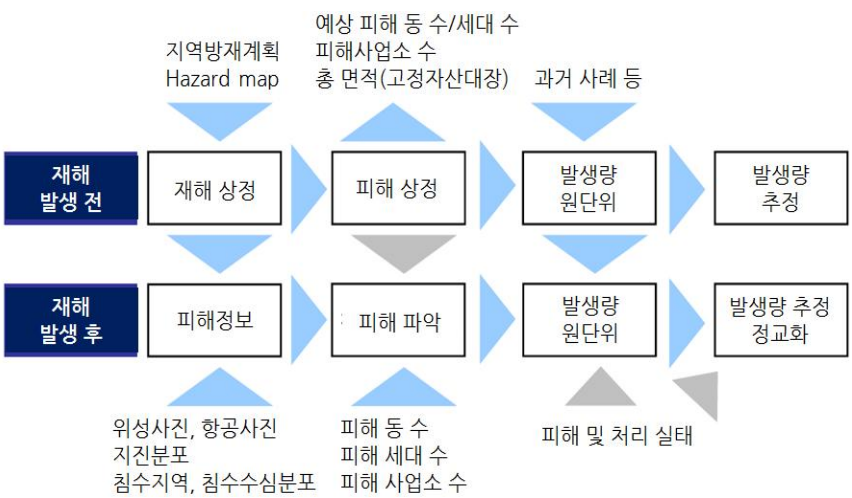

Figure 10 Estimation sequence of disaster waste generation amount (環境省大臣官房廃棄物·リサイクル対策部, 2014;016)

density, and four flood damage cases that occurred in Taiwan were analyzed. The result showed a close correlation between waste generation and population density, total precipitation, and flood damage area.

Table 2 Formula for estimating disaster waste generation amount

	predictive-generated Equation	P-value	R^2
Log transformation	log y = -4.137+0.718 log x1+0.600 log x2+1.422 log x3	logx1 : 0.0029, logx2 : < 0.0001, logx3 : 0.0113, log a : 0.0096	0.538
Exponential function	y=7.29×10-5×x10.718×x20.600 ×x31.422		
Log transformation	log y=-3.7291+0.5989 log x4+1.3956 logx3	logx4 : 0.0127, logx3 : < 0.0001, log a : 0.0113	0.541
Exponential function	y=1.866×10-4×x40.5989×x31.422		

Chen et al.(2007), Jo et al., 2016

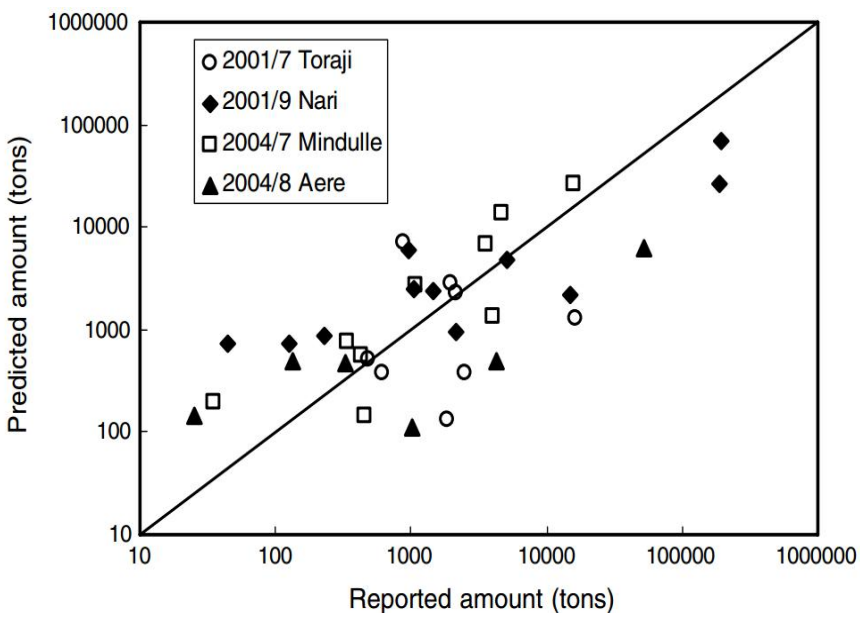

Figure 11 Comparison of estimated and actual disaster waste generation amounts (Chen et al., 2007)

In Korea, disaster waste quantity is predicted with reference to the information such as unit waste generation per waste type, density (weight per unit volume), and area of waste generation in the affected area, while the data of past ten years regarding waste quantity, level of damage, and weather observation data are used as well. When the waste quantity is predicted in this way, decisions can be made on the plans for collection and transportation as well as the number of temporary storage sites.

Disaster waste quantity varies according to the type of disaster and the affected area; in particular, the quantity of waste generated by a large-scale disaster is difficult to estimate in practice. Nevertheless, for rapid and accurate response upon a large-scale disaster event, estimation of waste quantity is a prerequisite. In line with this need, models and indicators have been developed globally for estimating disaster waste quantity before disaster occurs, to be used in actual disaster events, but the accuracy has been persistently questioned.

In countries such as the U.S., Japan, Taiwan and Australia, the estimation of disaster waste primarily relies on unit waste generation although it is hard to say that the circumstances and characteristics of the affected area were adequately reflected. In the case of Japan, when a disaster occurs, satellite images or aerial photos are acquired, then using the GIS or others, the level

of damage is analyzed. Based on unit waste generation, waste quantity estimation becomes more elaborate. However, a drawback of using satellite or aerial images is the difficulty of their acquisition in the right time of need, which requires complementary measures. Thus, despite the gravity of rapid and accurate disaster waste quantity estimation for appropriate disaster response, the measurement methods require further discussion.

III. Materials and Methods

The aim of this study was to construct a 3D spatial information using UAS and examine the feasibility of calculating waste amounts by computing the volume. After confirming the feasibility of calculating waste amounts, this approach was compared to terrestrial laser scanning (TLS) technology which shows high accuracy and has mainly been used to construct 3D spatial information in the past.

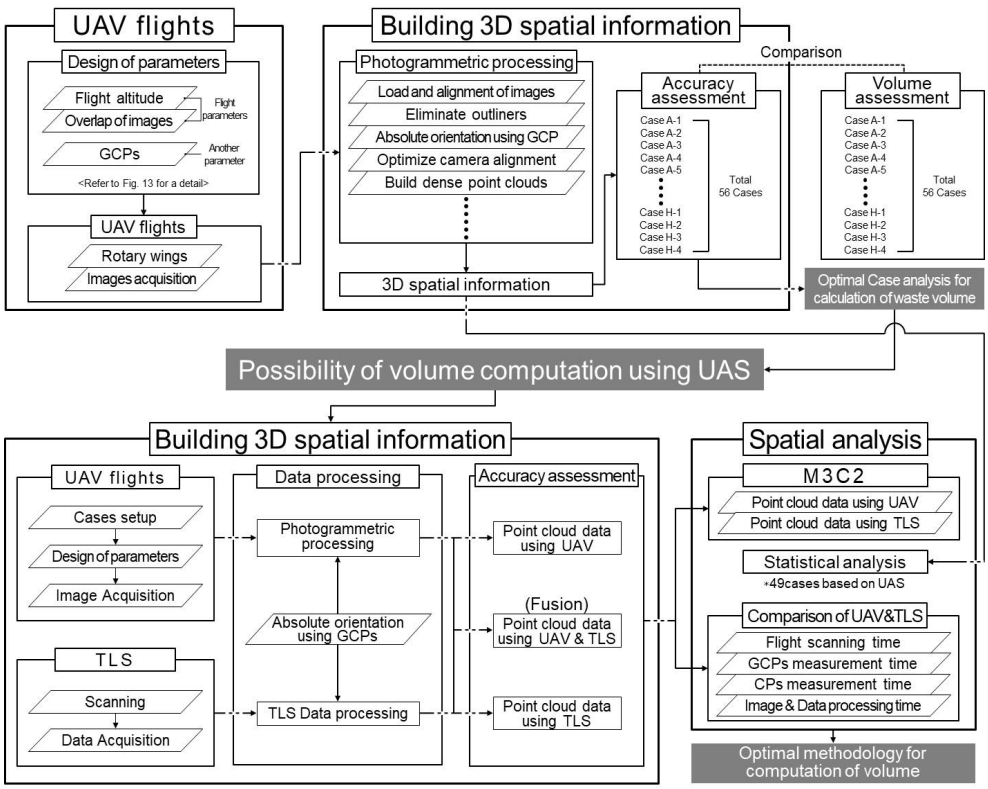

Figure 12 Process workflow

The two technologies were analyzed in terms of space and efficiency, and they were combined to produce an optimal waste calculation methodology. Figure 12 shows an overall flowchart of the study. The material used in the study is shown in Table 3.

Table 3 Research materials

Classification	Model	Specification
TLS	Leica Stanstation P40	Measurement type: time-of-flight Wave length: 1550nm (invisible) / 658nm (visible) Beam divergence: 0.23 mrad Beam diameter at exit: 3.5 mm Maximum range: up to 180 m at 18% reflectivity Scan rate: up to 1 000 000 points s^{-1} Highest resolution: 0.8 mm at 10 m
UAV & Camera	DJI Inspire1 Pro (T600)	Weight: 3.4kg(including camera and battery) Max speed: 18m/s Flight time: about 15m(18m tb48 battery)
	Zenmuse X5	Sensor Size: 17.3 x 13.0 mm (MFT: Micro Four Thirds) Max-Pixels: 16.0M Diagonal FOV: 72 degree Shutter Speed: 8~1/8000 sec Weight: 530g
VRS-RTK GNSS	Trimble R8s GNSS	440 channel GPS- and GLONASS-enabled VRS H: 8mm+0.5ppm RMS VRS V: 15mm+0.5ppm RMS
Data processing Software	Pix4D Mapper	Version 4.3
	Cyclone	Version 9.2.1
	CloudCompare	Version 2.10.2
	ArcMap	Version 10.1

1. Optimal Flight Parameters for UAV Generating 3D Spatial Information

1.1. Design of UAV Flight

This study developed a quick and accurate method for estimating the amounts of debris generated during disasters and waste generated during construction or civil engineering works. In real disaster zones, time and space cannot be controlled artificially. Accordingly, this study selected a study area where a large volume of spoil and various types of waste accumulated. It was located near the Namhan River, which flows southeast to northwest in Yeoju-si, South Korea. This area includes scenic views and an excellent-quality natural environment. The large-scale waste accumulated at the study site has caused many problems, not only damaging the scenic beauty of the site but also generating pollutants that flow into the river when it rains. Moreover, winds transport dust and odors from the waste site to nearby residential areas. An accurate estimation of the waste is required to dispose of it effectively. As the area is about 50,000 m^2, the large-scale accumulation of waste is challenging to measure.

Although it is hard to apply an actual waste area after natural disaster for the purpose of this study, an area with accumulated solid waste was selected.

Even though voids of solid waste will make difference, it will vary greatly depending on the characteristics of disaster area. In this study, wastes at the study site were regarded as wastes generated during disasters.

To construct 3D spatial information using an UAS, flight altitude and image overlap are the main parameters that need to be set. The number of GCPs are also reflected in the images. Following such developments, this study applied different flight altitudes, image multiplications, and number of GCPs to create various cases (Fig. 13).

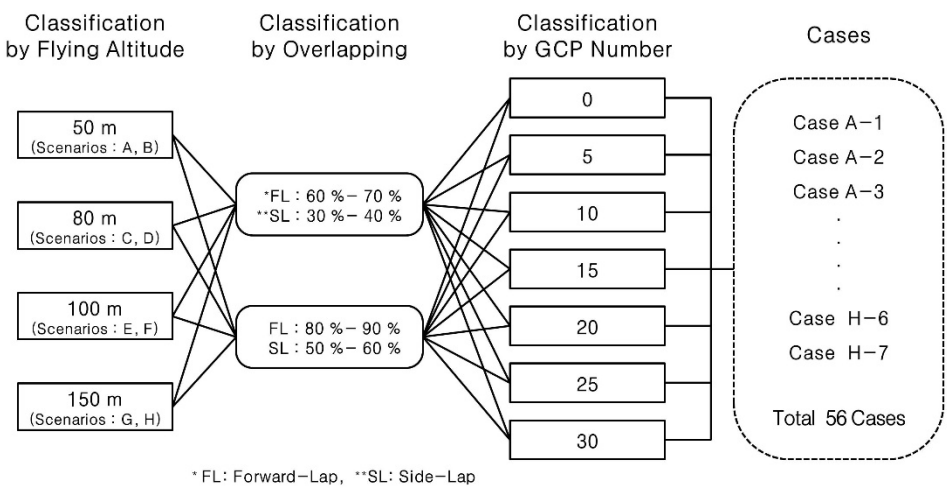

Figure 13 Design of UAV flight and Scheme for cases

Flight altitude directly affects the ground sampling distance (GSD). With regard to spatial resolution, GSD is the real pixel size, or the distance on

Earth between two adjacent pixels in an image. GSD can be obtained from the flight altitude, pixel size, and focal distance, as shown in the equation:

$$L_{\mathrm{GSD}} = \frac{d_{\mathrm{PS}} \times H}{f} \quad \text{(Eq. 7)}$$

where L_{GSD} is the GSD, d_{PS} is the pixel size, H is the flight altitude, and f is the focal distance.

While the pixel size and focal distance vary according to the type and performance of the camera, flight parameters can be set arbitrarily. Flight altitude determines the image resolution. In this study, four flight altitudes were set (50, 80, 120, and 150 m) to calculate the flight time and accurately estimate the waste amount.

Image overlap indicates how much an object taken in one picture is expressed by an adjacent image. When 3D spatial information is created from two-dimensional (2D) pictures, overlapping (stereo) pictures are needed; this will affect the accuracy of 3D spatial information. The overlap is classified into forward lap (FL) and side lap (SL). Here, FL was set to 60%–70% or 80%–90%, and SL was divided into 30%–40% or 50%–60%. The 10% gap in both subdivisions was based on the fact that the overlap

was not identified exactly when the real pictures taken by the UAV were analyzed. For example, when FL was set to 60% as one of the flight parameters for the UAV, not all the adjacent pictures had exactly 60% of FL with each other. This was because the surrounding environment (e.g., topographic features and weather) varied during every flight.

Along with the flight parameters, measuring GCPs is also important for inputting accurate location information into an image. In cases where only the GPS data from an UAV were used, without GCPs, to build a DSM or DEM, real measurements showed differences of over 20 m (Yoo et al. 2016). Studies on the number of GCPs and the location of measurements have been performed; however, no definitive criteria have been proposed. Existing studies have introduced various criteria such as allocating GCPs uniformly (Aber et al. 2010) or allocating 15 or more GCPs to ensure high accuracy (Coveney and Roberts 2017). This study considered both cases (applying and not applying GCPs). When applying GCPs, virtual reference station real-time kinematic-GNSS (VRS/RTK-GNSS) was used to classify 5, 10, 15, 20, 25, and 30 GCPs. Thus, the differences in elevation could be considered with the allocation of GCPs, and GCPs were measured at the highest, middle, and lowest elevations. The study area and the GCP measurement sites are shown in Figure 14.

In general, camera calibration minimizes image distortion. The three-dimensional model with camera calibration may have a higher accuracy than the three-dimensional model with self-calibration using aerial triangulation software (Pérez et al. 2013; Gašparović and Gajski 2016; Yu et al. 2017). However, Yu et al. (2017) found that the accuracy of the camera calibration-based three-dimensional model was slightly higher than that of the self-calibration-based three-dimensional model, but almost similar.

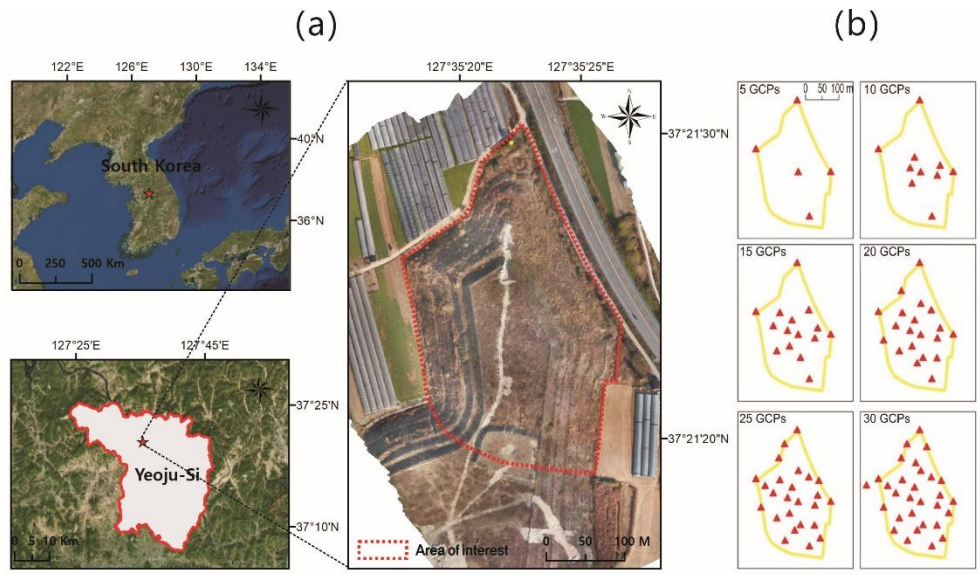

Figure 14 (a) Location of the study area and (b) Measuring points of ground control points

It is important to estimate the amount of waste in a relatively short period of time when estimating the amount of large-scale waste generated by

natural disasters as in this study. In addition, calibration of non-metric cameras, such as cameras attached to UAVs, is very sensitive to temperature and humidity. The environment during photographing and the environment during camera calibration in a laboratory may be different (Jeong 2011). When considering this fact and prioritizing urgency, it may be better to perform an UAV measurement using self-camera calibration rather than precise camera calibration. In the presents study, self-camera calibration provided by the Photoscan software was used, and the calibration results for each case were presented. Since the influence of the gimbal which connects the UAV and the camera when capturing the image is also an important variable, the effect of the gimbal for each case was also examined. Gimbal has three axes, but only roll and pitch axes were considered in this study (Gašparović and Jurjević 2017).

1.2. Photogrammetric Processing for the Acquisition of 3D Spatial Information

The obtained images were automatically registered by the SIFT and SfM algorithms to create 3D spatial information with 3D coordinates. The images were processed using the Photoscan software version 1.4.2.

Image processing consisted of the following six steps:

Step 1: Retrieve photographs captured by the UAV and arrange them based on key points and descriptors generated using the SIFT algorithm, with sparse point clouds produced using the bundler.

Step 2: Eliminate points determined to be outliers among the spare point clouds produced after arrangement.

Step 3: Match the coordinate system of the object using GCPs. In this process, after the GCP data measured at the site are entered, GCP markers are placed and matched onto the image with the captured GCPs.

Step 4: The camera arrangement optimization process extracts residuals between the GCPs and photographic reference points by performing aerial triangulation (Siebert and Teizer 2014) based on the entered GCPs.

Step 5: Produce point clouds in which individual points have their own x, y, and z values, using shape restoration techniques such as Clustering view for Multi-View Stereo (CMVS) and Patch-based Multi-View Stereo 2 (PMVS2), and absolute orientation values based on previously performed work.

Step 6: Produce DSM and orthographic images using the point clouds. The latest commercial software used to build 3D spatial information

includes an automatic camera calibration function. However, researchers often calibrate the camera manually for better accuracy (Yu et al. 2017). However, since one of the main objectives of this study was to build 3D spatial information quickly, the camera was self-calibrated.

1.3. Assessment of the 3D Spatial Information Accuracy

If the accuracy of the 3D spatial information is assessed, the amount of waste can be calculated accurately. Accuracy can be assessed by comparing the 3D spatial information constructed and GNSS reference data measured precisely at the site to extract the RMSE. The RMSE is a recognized and relatively easily understood proxy when a 'ground truth' dataset is a set of distributed points rather than a continuous 'truth' surface (Harwin and Lucieer 2012). In this study, check points (CPs) were measured to acquire the reference data and the VRS/RTK-GNSS used was the Trimble R8s.

For accuracy assessment, the reference data were acquired by performing measurements at CPs placed at 5 m intervals on two profiles across the study area (Fig. 15).

Profile A-A' had 59 CPs and Profile B-B' had 50 CPs, for a total of 109 CPs measured. The RMSE was calculated for the acquired reference data

and 3D spatial information produced for each case using Equation 2. In this case, the reference data and individual 3D spatial information points have their own x, y, and z values; therefore, these values of the RMSE, and the xy (2D) and *xyz* (3D) values, were also compared and analyzed.

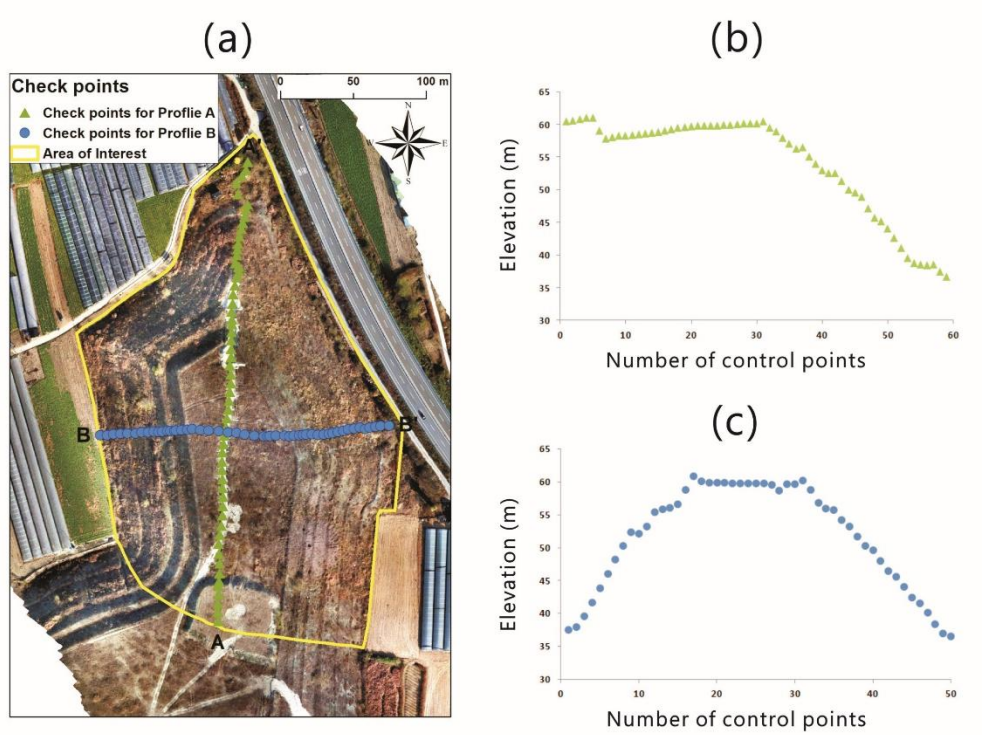

Figure 15 Measurement of CPs using VRS/RTK-GNSS: (a) Check points, (b) Check points for Profile A-A' and (c) Check points for Profile B-B'

In this study, the RMSE values obtained from Equations 8–12 are analyzed and discussed and the x, y, and z values are presented as *xyz* (3D) in the equations below:

$$(RMSE)_x = \sqrt{\frac{\sum_{i=1}^{n} \Delta x_i{}^2}{n}} \quad \text{(Eq. 8)}$$

$$(RMSE)_y = \sqrt{\frac{\sum_{i=1}^{n} \Delta y_i{}^2}{n}} \quad \text{(Eq. 9)}$$

$$(RMSE)_z = \sqrt{\frac{\sum_{i=1}^{n} \Delta z_i{}^2}{n}} \quad \text{(Eq. 10)}$$

$$(RMSE)_{xy} = \sqrt{(RMSE)_x{}^2 + (RMSE)_y{}^2} \quad \text{(Eq. 11)}$$

$$(RMSE)_{xyz} = \sqrt{(RMSE)_x{}^2 + (RMSE)_y{}^2 + (RMSE)_z{}^2} \quad \text{(Eq. 12)}$$

where (RMSE)x, (RMSE)y, (RMSE)z, (RMSE)xy, and (RMSE)*xyz* are the x, y, z, xy (2D) and *xyz* (3D) RMSE values, respectively; Δxi, Δyi, and Δzi are the differences between the reference coordinates and the coordinates determined from the point cloud; and n is the number of points.

1.4. Computation of the Amount of Waste

Since the majority of the waste was concentrated at the bottom of the heap and there was less waste in the upper part, it was necessary to make a clear distinction between the heap of waste and the surface of the ground. The VRS/RTK-GNSS method was used to identify the boundary between

the ground and the waste at the study site before calculating the amount of waste.

In this study, the waste quantity is the volume of 3D spatial information. In the DSM constructed in Step 6 of the photogrammetric processing, the volume per cell can be calculated. The volume computation formula for a single cell (V_i) is as follows:

$$V_i = L_i \times W_i \times H_i \quad \text{(Eq. 13)}$$

where L_i, W_i are the length and width of the cell, and H_i is the height of the cell (Raeva et al., 2016).

The accuracy of the volume was affected directly by the accuracy of the x, y, and z coordinate values on the surface, point distribution, and number of GCPs (Yilmaz et al., 2010; Rhodes, 2017). In other words, the volume can be accurately estimated when the 3D point cloud is constructed at the correct position. In previous studies that calculated volume based on 3D point clouds (Yilmaz, 2010; Hugenholtz et al., 2015; Rhodes, 2017), the accuracy of the volume was assessed using the RMSEs of the x, y, and z coordinates. In this study, the waste quantity, given as 3D spatial

information, was calculated for all cases and their relationship with the position accuracy was examined.

2. Comparison and Analysis of TLS and UAS Methodology for Optimal Volume Computation

Firstly, Two point clouds were built using TLS and UAS technologies separately, evaluated their accuracies, and performed volume computation. For the UAS investigation, Various cases were set and performed volume computation for the case yielding the most accurate point cloud. Then, conducted comparative special analysis of the TLS and UAS technologies and performed volume computation with a TLS/UAS fusion model. Finally, the volume was analysed computation results.

As the study area, a bulky waste disposal site in Jipyeon-ri in Sejong City was chosen. Sejong City is a planned city in which large construction sites and residential areas coexist. Excavated earth materials and construction waste are piled up at a temporary waste disposal site, not only damaging the landscape, but also posing problems to residential areas via wind-blown dust. Construction site waste management is therefore a compelling issue, and accurate waste volume computation is important for planning waste clearing.

The waste disposal site selected as the study area extends over about 6,000 m^2, with a huge amount of waste accumulated on it, making it a great challenge to measure the total amount (Fig. 16).

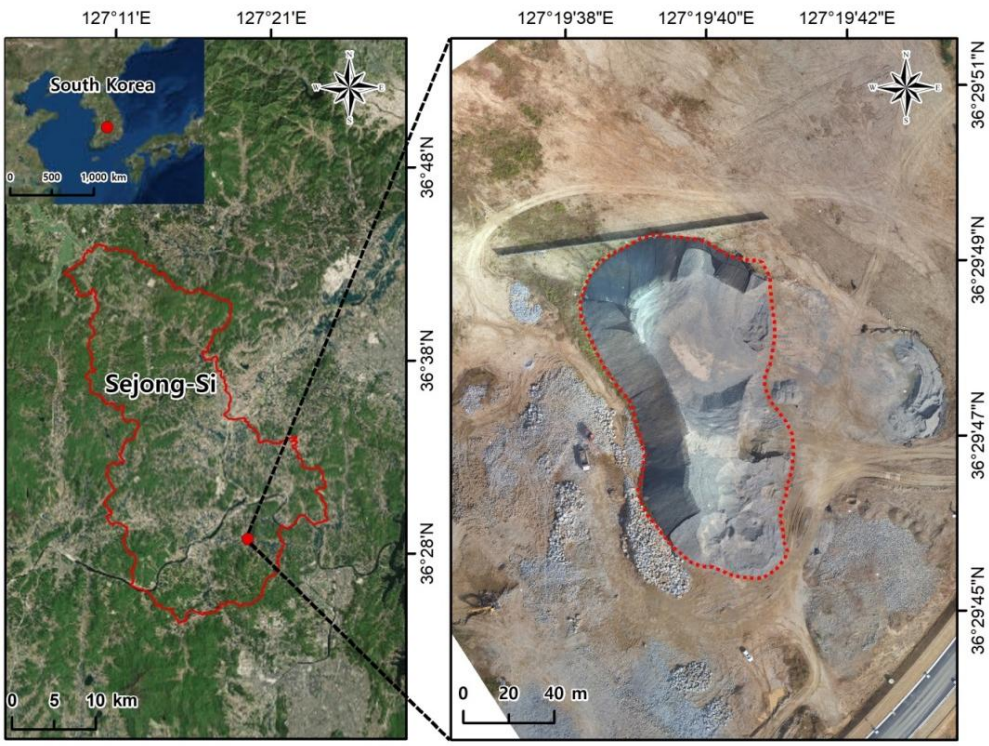

Figure 16 Location of the study area (chapter 2 &3)

2.1. TLS and UAS-based 3D Spatial Information Generation and Volume Computation

The overall process of TLS-based point cloud generation can be largely divided into three phases. Firstly, in the goalsetting and planning phase, the scan positions and distances should be planned taking into account shadow zones and disturbances.

Secondly, in the field scanning phase, scanning is performed from the planned scan positions and backup is executed to prevent data loss. The quality of the scanned data is also checked during scanning, and rescanning is performed if necessary. In this study, field scanning was conducted at 20 scan positions (Fig. 17). To ensure accurate registration of individual scan data, GCPs should be measured in the survey area and the measured values should be reflected in the ensuing data processing. Four GCPs was set four GCPs in study area.

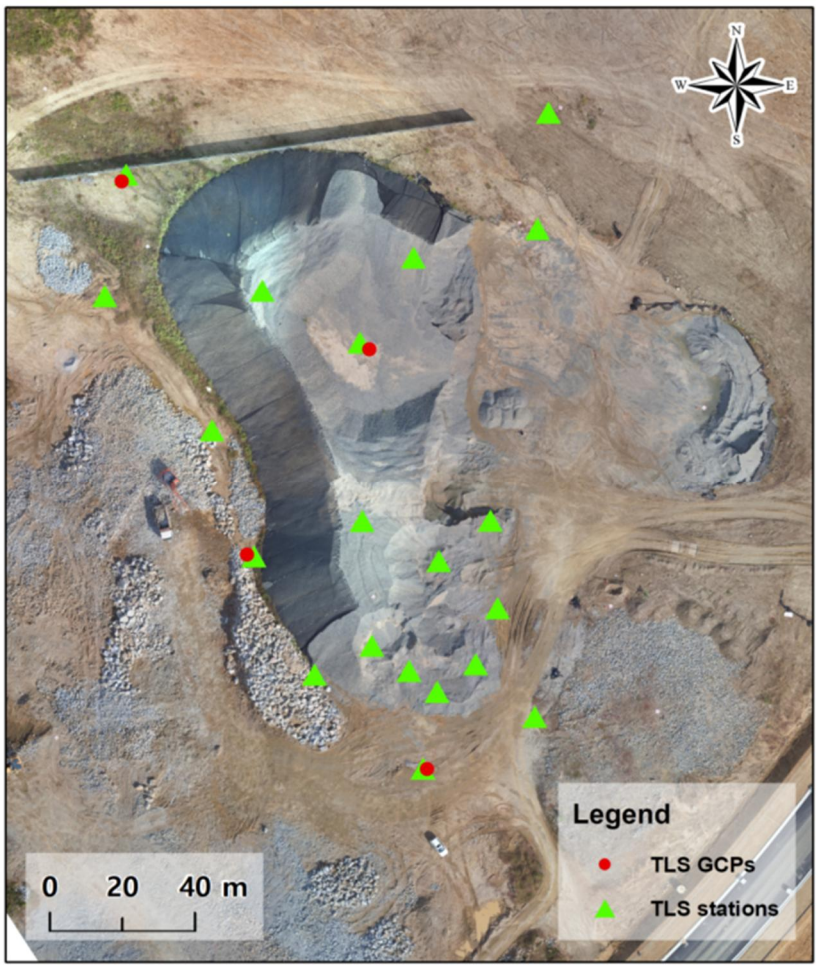

Figure 17 TLS scan positions and GCPs

Thirdly, in the data processing phase, the datasets acquired in the field scanning phase are registered and converted into georeferenced coordinates. The converted data points are realigned, and unnecessary parts are removed.

Data processing was performed using Cyclone 9.2.1 software, and accuracy evaluation and volume computation were conducted using

CloudCompare 2.10.2 and ArcMap 10.1 software, respectively.

To implement UAS-based point cloud generation, Flight altitude was set the flight altitude, image overlap, and number of GCPs as key parameters. The flight altitude was varied from 40 to 160 m in intervals of 40 m. A higher flight altitude can reduce the flight time by reducing the number of images required to cover the survey area but results in a larger ground sampling distance, i.e., lower image resolution and, consequently, lower quality. Therefore, the flight height was set to four different levels taking into account the height of the waste pile in the survey area. Greater image overlap can enhance the quality of image registration results but requires more flight and data processing time. Fairly high overlap was set: 85% forward lap and 65% side lap.

The number of GCPs is an important parameter related to image quality, and many studies have been conducted to clarify the relationship between the number of GCPs and image quality enhancement. According to one study, one GCP per 2 ha yielded the highest accuracy (Coveney and Roberts, 2017), and another study highlighted the importance of an even distribution of GCPs across the survey area (Aber et al., 2016). Based on the results of previous studies, a sufficient number of GCPs were set up to examine the association between the the number of GCPs and the point cloud accuracy.

This was done by conducting two surveys in two GCP placement cases, placing 10 GCPs across each survey area, one of which included the waste pile while the other excluded it (Fig. 18). This GCP placement criterion is different from those of previous studies in which more importance was given to the number of GCPs or their even distribution. Different criterion was used to test our hypothesis that altitude-dependent GCP placement would influence the image quality.

Data processing was performed using Pix4d Mapper 4.3 software, and accuracy evaluation and volume computation were conducted using CloudCompare 2.10.2 and ArcMap 10.1 software, respectively.

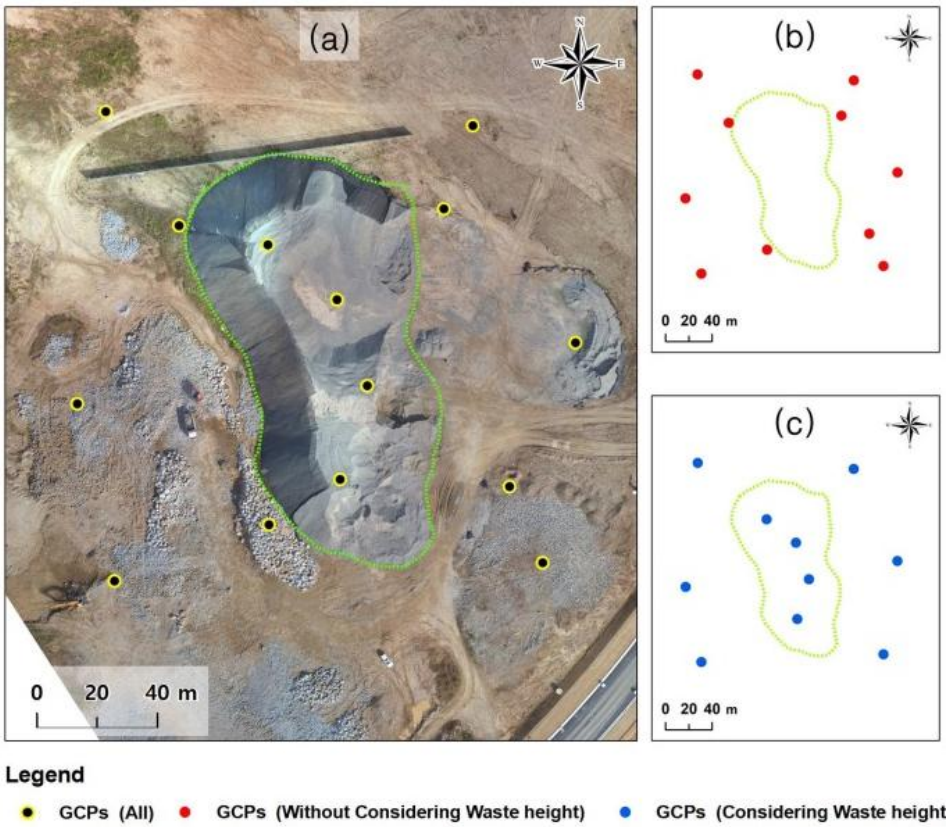

Figure 18 GCP positions: (a) all GCPs; (b) GCPs placed without considering waste height; (c) GCPs placed considering waste height.

The accuracies of the point clouds generated using TLS and UAS technologies were evaluated by comparing them with those generated by setting a large number of CPs in the survey area based on a GNSS field survey. The RMSE was used as a measure of accuracy. The RMSE is a recognized and relatively easily understood proxy when a "ground truth" dataset is a set of distributed points rather than a continuous "truth" surface

(Harwin and Lucieer, 2012). In this study, CPs were measured with the VRS/RTK-GNSS in the Trimble R8s.

In total, 311 CPs were measured, as shown in Fig. 19.

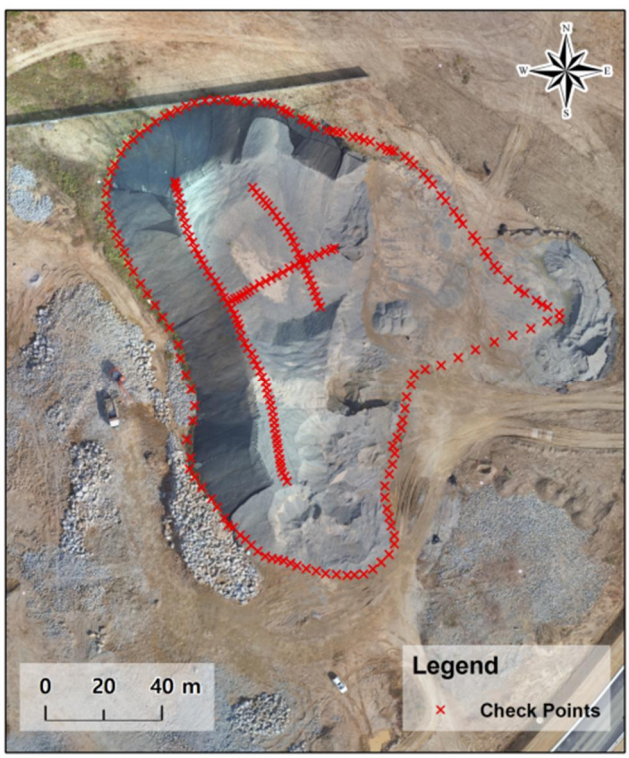

Figure 19 CP positions

Measurements were performed at CPs located across the study area, generating reference data essential for evaluating the point cloud accuracy. The RMSE basically reflects the accuracy of each of the x, y, and z components, but RMSE was computed using the *xyz* value, which was

obtained by combining the RMSEs separately corresponding to x, y, and z.

2.2. Comparison and Analysis of 3D Spatial Information

Point clouds were compared generated using the two above-mentioned technologies by analyzing their spatial features and efficiencies. Three techniques are generally used when comparing two spatial models: the DEM of difference (DoD), direct cloud-to-cloud (C2C), and cloud-to-mesh or cloud-to-model distance (C2M) techniques (Barnhart and Crosby, 2013; Lague et al., 2013). However, these methods have their respective drawbacks when employed to compare point clouds, which can be summarized as follows:

The DoD method, which is used to compare two DEMs, cannot cope with overhanging and the information density decreases proportionally to the surface steepness (Barnhart and Crosby, 2013). Moreover, it is not a full 3D spatial information, but rather a 2.5D model adding z to a cell, making it unsuitable for evaluating the complex morphologies of solid wastes (Yu et al., 2018).

The C2C approach is the simplest and fastest direct method of 3D comparison of point clouds (Girardeau-Montaut et al., 2005). For each point

of the second point cloud, a closest point can be defined in the first point cloud. In its simplest version, the surface change is estimated as the distance between the two points. However, this method cannot be used to calculate spatially variable confidence intervals (Lague et al., 2013).

In the C2M method, the surface change is calculated based on the distance between a point cloud and a reference 3D mesh (Cignoni et al., 1998). It generally requires time-consuming manual inspection. As is the DoD technique, interpolation over missing data introduces uncertainties that are difficult to quantify (Lague et al., 2013).

To overcome these uncertainties associated with spatial data comparison, the Multiscale Model to Model Cloud Comparison (M3C2) algorithm can be employed (Lague et al., 2013). The M3C2 algorithm has been used because it enables rapid analysis of point clouds with complex surface topographies (Barnhart and Crosby, 2013; Lague et al., 2013; James et al., 2017; Yu et al., 2018). The M3C2 algorithm finds the best-fitting normal direction for each point, then calculates the distance between the two point clouds along a cylinder of a given radius projected in the direction of the normal (Cook, 2017). In this study as well, point cloud comparison was performed using the M3C2 algorithm instead of a conventional spatial model comparison technique.

3. Multispace Fusion Methodology-based 3D Spatial Information Generating and Efficiency Analysis

3.1. Multispace Fusion Methodology-based 3D Spatial Information

One point cloud was built by fusing the TLS- and UAS-based point clouds to compare the spatial accuracy and efficiency of the TLS-UAS fusion model with those of each individual model and analyzed the comparison results. Although higher accuracy was expected of the point cloud generated using the fusion model, it was also necessary to consider the efficiency. Two technologies was fused and analyzed the performance of the fusion method to test the hypotheses that the TLS- and UAS-based point clouds have their respective problems and that those problems can be solved by point cloud generation using a method in which these two technologies are fused. As the UAS-based point cloud, The most accurate was selected one from among the eight point clouds generated according to eight different cases.

The TLS- and UAS-based point clouds were fused using CloudCompare 2.10.2 software. Since they use the same coordinate system (Korea 2000/Central Belt 2010-EPSG:5186), there is no need to perform additional

geo-referencing.

The volume computation accuracy of the point cloud generated by the fusion approach was evaluated using the same method that was employed for the TLS and UAS methods.

3.2. Efficiency Analysis of 3D Spatial Information for Responding to Large-scale Disasters

For efficiency analysis, The time was employed variables used by Silva et al. (2017) when comparing UAS, GNSS, and LiDAR and those used by Son et al. (2018) when building a UAS-based DSM. In order to construct 3D spatial information from the waste area in Yeojoo city, Chapter1 performed a analysis on total elapsed time and accuracy and compared the 3D spatial information based on UAS and the 3D spatial information based on TLS from waste area in Sejong city in terms of elapsed time and accuracy of.

In addition to time, the efficiency was analyzed using all costs spent to construct the 3D spatial information by using the two technologies.

III. Result and Discussion

1. Optimal Flight Parameters for UAV Generating 3D Spatial Information and Investigation of Feasibility

1.1. Generation of 3D Spatial Information using UAS

Several images were obtained according to various flight parameters. Fifty-six 3D spatial information sets were analyzed based on a total of fifty-six flight cases. The cases were classified from A to H according to flight altitude and overlap and were subdivided by the number of GCPs.

In this study, seven cases with the lowest flight altitudes and low levels of overlap were not registered and spatial information from the remaining 49 cases was analyzed.

Generally, GSD—L_{GSD} in Equation (1)—decreased as the flight altitude decreased, and images had a higher resolution. However, if there were large differences in elevation at a site, registering images was impossible at lower altitudes. The flight altitude, elevation of an object, and above-ground level (AGL) are described in Figure 20.

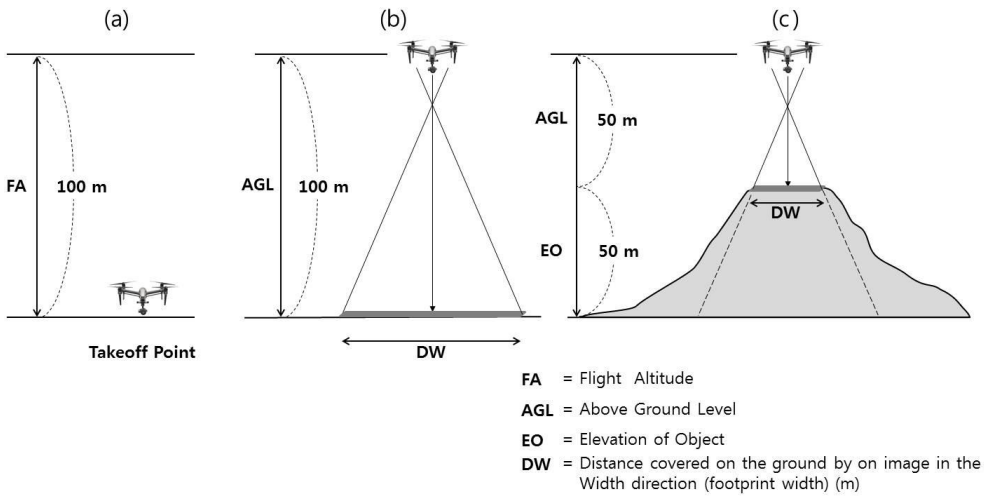

Figure 20 DW variation of the target site for the UAV according to the altitude: (a) Takeoff point, (b) Above Ground Level and (c) Distance covered on the ground by on image in Width direction

In Figure 20, a is the UAV takeoff point and height. When setting the UAV takeoff height to 100 m, an altitude of 100 m while photographing the object is maintained. In the case of objects located at a high altitude, such as those in this study area, it is difficult to climb with an UAV, so takeoff should be performed at a low altitude. In Figure 20, b is AGL, which means the distance from the surface to the UAV. The AGL changes according to the altitude of the ground. At the UAV takeoff point, the flight altitude and AGL height are the same. However, when the elevation of an object is 50 m in c in Figure 20, the AGL also becomes 50 m. In other words, the higher the elevation of an object, the lower the AGL. When the AGL is lowered, the distance covered on the ground by an image in the width direction (DW),

which is the UAV photographic area, decreases. When the DW is small, there is no overlap between the captured images, so the images may not match as shown on the left side of Figure 21.

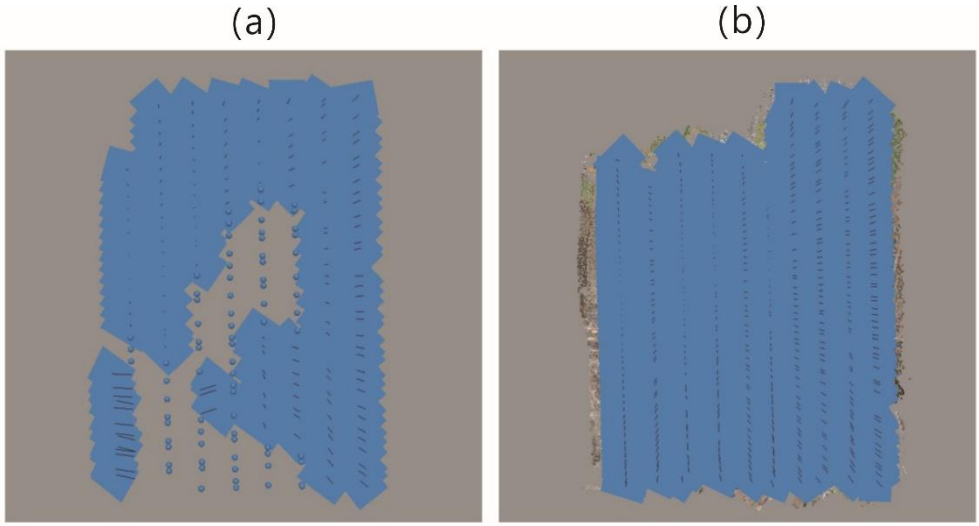

Figure 21 (a) Case A with unregistered images and (b) case D showing the overall registration of images

The left side of Figure 21 is the case A. In case A, which involved a flight altitude of 50 m, FL was 60%–70% and SL was 30–40%; only 162 of the 237 images were registered while case D registered images for the entire area of the site.

A spatial analysis using the UAV data showed that large spaces can be analyzed quickly, and the flight time and number of images can be derived

according to the flight altitude (Mesas-Carrascosa et al. 2016). This study obtained the flight time, number of images, and GSD according to the flight altitude and overlap (Table 4).

Table 4 GSD, UAV flight time, and number of images according to flight altitude and overlap

Flight altitude (m)	Overlap							
	FL: 60%–70%/SL: 30%–40%				FL: 80%–90%/SL: 50%–60%			
	Case	GSD (cm)	Flight time (min)	Number of images	Case	GSD (cm)	Flight time (min)	Number of images
50	A	-	11’	162/237	B	1.91	46’	934/934
80	C	3.38	6’	118/118	D	3.28	20’	489/491
120	E	5.11	4’	69/69	F	5.16	9’	217/217
150	G	6.70	3’	46/46	H	6.62	4’	86/86

The results showed that the GSD tended to increase as the flight altitude increased, as described in Equation 7, but it was below 10 cm in every case. On the other hand, the overlap had little effect on the GSD.

Table 5 shows the camera interior orientation parameters for all cases except case A that was not matched. The parameters were divided into focal length, principal point, radial distortion, and tangential distortion, and the values were described.

Table 5 Camera interior orientation parameters

Case	Focal length (F)	Principal point (Cx/Cy)	Radial distortion (K1/K2/K3)	Tangential distortion (P1/P2)
B	4036.59	51.71/–0.56	0.0128/–0.0782/0.2176	0.0027/0.0004
C	4118.69	34.25/–22.16	0.0171/–0.1328/0.3869	0.0032/0.0008
D	4070.11	53.33/10.81	0.0106/–0.0769/0.2175	0.0026/0.0005
E	4074.98	57.28/9.20	0.0237/–0.1743/0.5249	0.0029/0.0012
F	4037.26	54.86/7.09	0.0088/–0.3506/0.0488	0.0024/0.0005
G	4042.66	82.26/22.20	0.0031/–0.0012/0.0290	0.0041/0.0007
H	4050.14	58.37/5.26	0.0071/–0.0308/0.0466	0.0028/0.0002

Table 6 shows the statistical values for gimbal axes for each case.

Table 6 Statistical values of gimbal axes for each case

Case	Avg		Std		Min		Max	
	Pitch(°)	Roll(°)	Pitch(°)	Roll(°)	Pitch(°)	Roll(°)	Pitch(°)	Roll(°)
B	–10.64	–20.67	47.37	82.05	–88.96	–91.81	86.14	90.53
C	1.23	9.16	34.37	34.86	–60.03	–61.8	66.87	62.76
D	–4.31	12.04	35.1	33.57	–66.01	–58.41	64.47	67.71
E	1.39	0.49	35.05	42.41	–67.16	–71.04	73.23	63.68
F	2.99	1.34	0.93	0.67	–1.54	–1.08	4.12	3.05
G	4.59	2.61	14.11	19.2	–22.52	–25.15	19.97	23.58
H	2.58	2.16	1.35	0.79	–2.69	–0.42	4.31	3.32

In all cases except case A where the images were not matched, the standard deviations of the pitch and roll decreased as the flight altitude increased. In addition, even at the same altitude, a low standard deviation value was confirmed in a high overlapping ratio of the image. For example, case G and H showed the same flight altitude of 150 m, but a low standard deviation value was found in case H with a high overlapping ratio.

1.2. Assessment of the 3D Spatial Information Accuracy

The spatial information x, y, z, xy (2D), and *xyz* (3D) RMSEs for each of the 49 cases were analyzed to verify their accuracy (Table 7); in this process, flight altitude, overlap, and number of GCPs were distinct. The *xyz* (3D) value of the RMSE was mainly used for the assessment.

Table 7 Accuracy of x, y, z, and *xyz* locations in each case

Case		RMSE (m)					Case		RMSE (m)				
		x	***y***	***z***	***xy***	***xyz***			***x***	***y***	***z***	***xy***	***xyz***
A	1	No 3D spatial information					B	1	0.57	1.38	105	1.5	105
	2							2	0.32	0.23	1.07	0.4	1.11
	3							3	0.09	0.11	0.62	0.14	0.63
	4							4	0.06	0.08	0.21	0.1	0.24
	5							5	0.05	0.06	0.14	0.08	0.17
	6							6	0.04	0.05	0.15	0.06	0.16
	7							7	0.04	0.06	0.19	0.07	0.2

C	1	1.73	1.81	121	2.5	121	D	1	0.47	1.01	124	1.12	124
	2	0.37	0.62	1.01	0.72	1.24		2	0.14	0.09	0.15	0.17	0.22
	3	0.22	0.28	0.6	0.36	0.7		3	0.1	0.05	0.13	0.11	0.17
	4	0.15	0.22	0.61	0.27	0.67		4	0.07	0.04	0.12	0.08	0.15
	5	0.09	0.11	0.25	0.15	0.29		5	0.05	0.05	0.08	0.07	0.11
	6	0.08	0.06	0.43	0.1	0.28		6	0.04	0.04	0.08	0.06	0.1
	7	0.09	0.07	0.43	0.11	0.29		7	0.05	0.03	0.06	0.06	0.08
E	1	0.59	1.43	121	1.54	121	F	1	0.39	1.36	123	1.41	123
	2	0.09	0.08	0.61	0.13	0.63		2	0.11	0.1	0.13	0.15	0.2
	3	0.11	0.16	0.21	0.2	0.29		3	0.1	0.06	0.1	0.12	0.16
	4	0.06	0.09	0.23	0.1	0.25		4	0.07	0.04	0.11	0.08	0.14
	5	0.06	0.06	0.19	0.09	0.21		5	0.04	0.04	0.13	0.06	0.15
	6	0.06	0.09	0.22	0.11	0.25		6	0.03	0.04	0.09	0.06	0.11
	7	0.06	0.07	0.2	0.09	0.22		7	0.04	0.06	0.1	0.07	0.13
G	1	0.61	2.41	125	2.48	125	H	1	1.91	2.65	124	3.27	124
	2	0.34	0.46	1.14	0.57	1.28		2	0.15	0.11	0.24	0.19	0.31
	3	0.12	0.12	0.28	0.17	0.33		3	0.06	0.07	0.11	0.09	0.14
	4	0.08	0.11	0.29	0.14	0.32		4	0.06	0.05	0.11	0.08	0.14
	5	0.1	0.15	0.22	0.18	0.29		5	0.05	0.05	0.11	0.07	0.13
	6	0.08	0.12	0.18	0.15	0.24		6	0.05	0.04	0.16	0.06	0.18
	7	0.06	0.05	0.12	0.08	0.15		7	0.05	0.04	0.21	0.06	0.22

Table 8 shows the value of each case parameters.

Table 8 Value of each case parameters

Case		Classification by Flying Altitude	Classification by Overlapping	Classification by GCP Number	*xyz* RMSE(m)
A	1	50m	FL: 60%–70% SL: 30%–40%	0	
	2			5	
	3			10	
	4			15	
	5			20	
	6			25	
	7			30	
B	1	50m	FL: 80%–90% SL: 50%–60%	0	105
	2			5	1.11
	3			10	0.63
	4			15	0.24
	5			20	0.17
	6			25	0.16
	7			30	0.2
C	1	80m	FL: 60%–70% SL: 30%–40%	0	121
	2			5	1.24
	3			10	0.7
	4			15	0.67
	5			20	0.29
	6			25	0.28
	7			30	0.29
D	1	80m	FL: 80%–90% SL: 50%–60%	0	124
	2			5	0.22
	3			10	0.17
	4			15	0.15
	5			20	0.11
	6			25	0.1
	7			30	0.08
E	1	100m	FL: 60%–70% SL: 30%–40%	0	121
	2			5	0.63
	3			10	0.29
	4			15	0.25
	5			20	0.21
	6			25	0.25
	7			30	0.22
F	1	100m	FL: 80%–90% SL: 50%–60%	0	123
	2			5	0.2
	3			10	0.16
	4			15	0.14
	5			20	0.15
	6			25	0.11
	7			30	0.13

G	1	150m	FL: 60%–70% SL: 30%–40%	0	125
	2			5	1.28
	3			10	0.33
	4			15	0.32
	5			20	0.29
	6			25	0.24
	7			30	0.15
H	1	150m	FL: 80%–90% SL: 50%–60%	0	124
	2			5	0.31
	3			10	0.14
	4			15	0.14
	5			20	0.13
	6			25	0.18
	7			30	0.22

First, to assess the accuracy of the 3D spatial information according to the flight altitude, the RMSE data for the same overlap and GCP number were analyzed (Fig. 22).

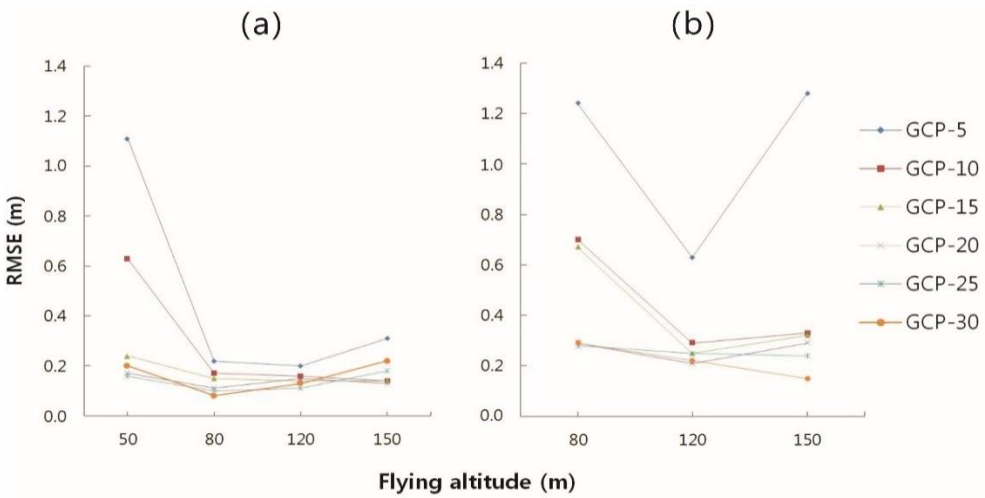

Figure 22 (a) RMSE with high levels overlap (FL : 80%- 90%, SL : 50%-60 %) an d number of GCPs to flight altitude and (b) RMSE with the low levels (FL : 60%-70%, SL : 30%- 40%) overlap and number of GCPs to flight altitude

Since images captured during flight at a 50 m altitude were not matched, the lowest flight altitude was 80 m. Most cases showed a high RMSE at the lowest flight altitude. However, some cases, which had as many as 25 or 30 GCPs, showed a high RMSE even at a flight altitude of 150 m. This needs to be discussed when accuracy is verified according to the number of GCPs.

Among 49 cases, B-5, D-5, F-5, and H-5 have been taken as examples for discussion. These cases had the same number of GCPs (20) and the same overlap (FL: 80%–90%, SL: 50%–60%), and the flight altitudes were 50, 80, 120, and 150 m, respectively. The RMSE values were 0.17 (B-5), 0.11 (D-5), 0.15 (F-5), and 0.13 m (H-5). The highest accuracy was produced at an altitude of 80 m, while the lowest was produced at an altitude of 50 m. Accuracy generally increases at low flight altitudes, but this study obtained the opposite results.

The accuracy assessment was conducted in terms of overlap, which was classified into two groups (FL: 60%–70%/SL: 30–40% and FL: 80%–90%/SL: 50%–60%). In every case, higher levels of overlap were associated with lower RMSEs (Fig. 23).

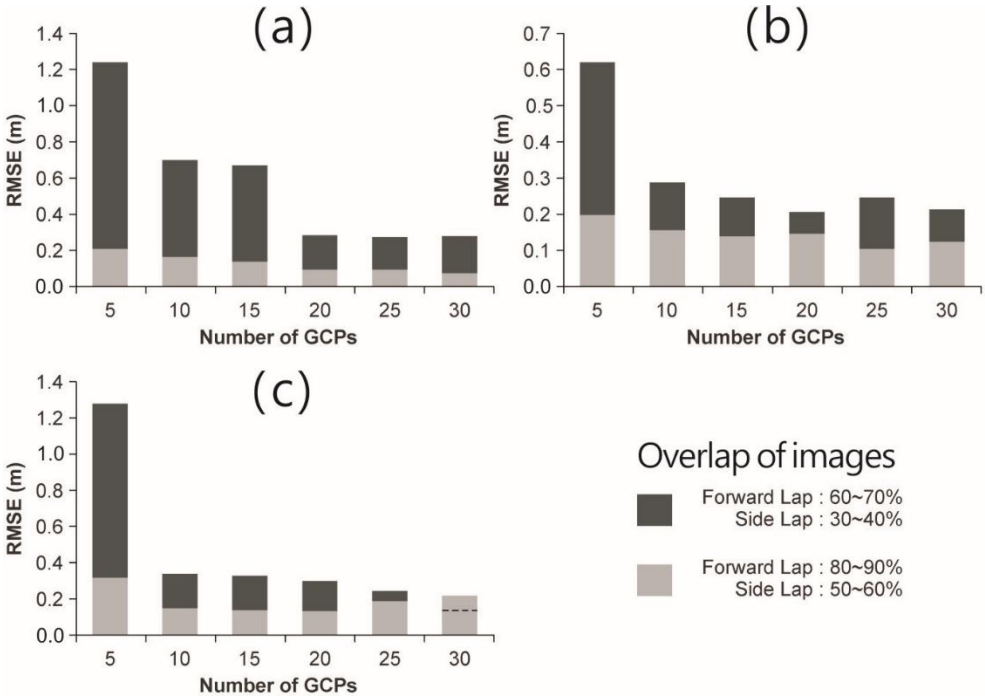

Figure 23 RMSE with the same flight altitude and number of GCPs according to ov erlap : (a) Flight altitude 80 m, (b) Flight altitude 120m, (c) Flight altitude 150m

Differences in RMSE were analyzed according to overlap when the flight altitude and number of GCPs were the same. The case with no GCPs was excluded from analysis because its accuracy was too low. The differences in FL and SL were set to 20% in both groups of overlaps, but the differences in accuracy when the flight altitude and number of GCPs were the same turned out to be variable. In every case, 3D spatial information obtained through the application of higher overlaps (FL: 80%–90% SL: 50%–60%) had low RMSEs, while 3D spatial information taken at an altitude of 150 m with 30

GCPs yielded the opposite result. The two overlaps showed that there was a large difference in the RMSE of the two overlaps particularly for five GCPs.

Finally, accuracy was analyzed according to the number of GCPs (i.e., when the same flight altitude and overlap were applied; Figure 24).

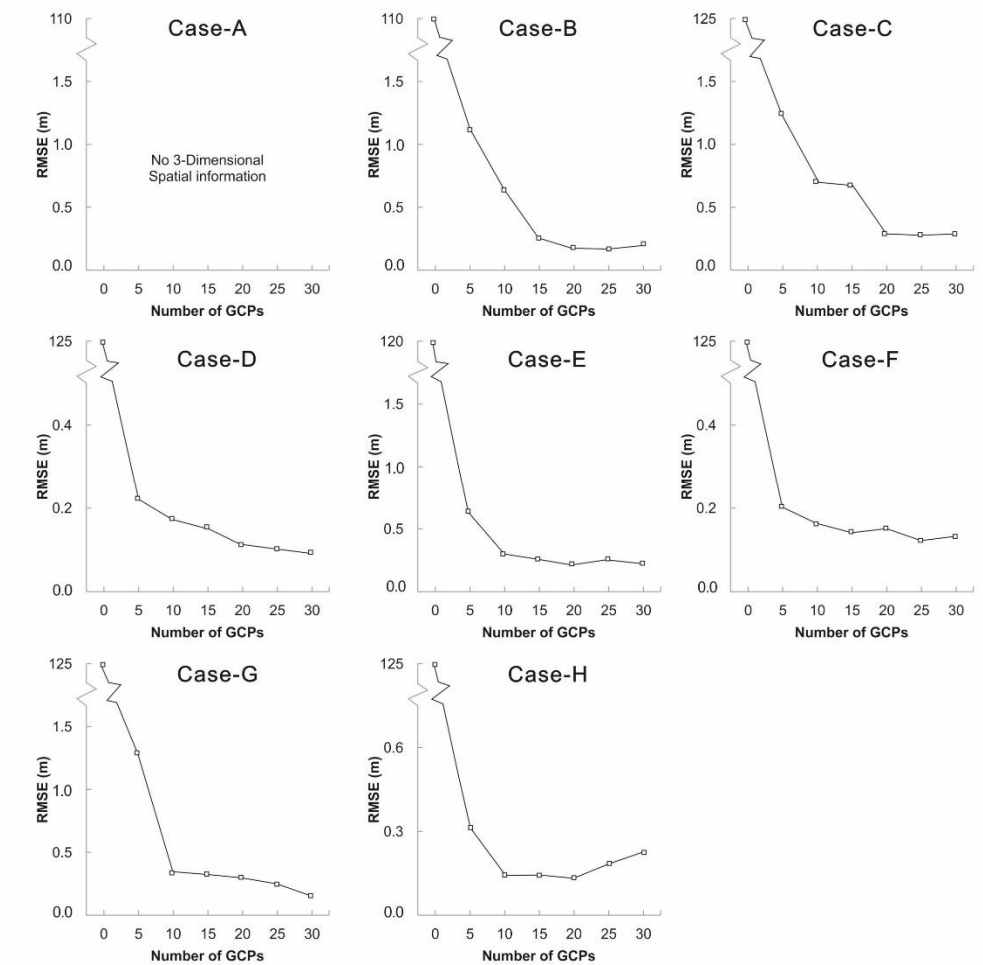

Figure 24 RMSE of each case according to the number of GCPs

As the number of GCPs increased from 0 to 30 in cases B to H, RMSE decreased. However, when the number of GCPs was 30, RMSE increased in some cases. There were other cases in which the variation in RMSE decreased as the GCPs started to converge to a certain number.

Case A could not be assessed since the images were not registered. However, it was possible to assess case B. Case B-1, in which no GCP was applied, had an RMSE value of about 100 m, which was indicative of very inaccurate locations. As the number of GCPs increased from 5 (B-2) to 10 (B-3) to 15 (B-6), the variation in the RMSE was high, but it decreased gradually. When there were 20 GCPs (B-5), the RMSE began to vary slightly. When there were 25 GCPs (B-6), the RMSE was at its lowest (0.16 m), and as the GCPs increased to 30 (B-7), the RMSE tended to increase slightly. Cases C, D, and E displayed a similar tendency. It is convention that as the number of GCPs increases, the RMSE decreases, indicating an improved accuracy. However, in this study, the RMSE tended to increase when the number of GCPs was the highest for a specific case. This seems to be related to location errors, which accumulated when several GCPs were used. In cases F, G, and H, the RMSE showed little variation as the number of GCPs increased beyond 10 or 15. In other words, as the flight altitude increased, the variation in the RMSE decreased for a few GCPs.

According to a previous study, the accuracy of 3D spatial information is affected by flight altitude more than by other parameters (Mesas-Carrascosa et al. 2016). Previous research on the relationship between flight altitude and accuracy of images also usually classified information with flight altitudes ranging from 30 to 120 m or higher, and with various image acquisition techniques. Some studies demonstrated similar accuracies even when different flight altitudes were applied. For example, an image taken at an altitude of 60 m by Uysal et al. (2015) had a similar vertical accuracy to that of one taken at 120 m by Agüera-Vega et al. (2017). Although the images could have contained different overlaps or GCPs, it is notable that such a similarity in accuracy was obtained from such a large difference in flight altitude.

This study also analyzed the accuracy of 3D spatial information for different flight altitudes with the same number of GCPs and the same overlap to assess accuracy according to the flight altitude. Previous studies have shown that accuracy generally increased as altitude decreased, but this study showed that accuracy was low at the lowest flight altitude. This appears to have been a result of the difference in DW caused by large differences in elevation in the target area. As shown in a in Figure 20, the UAV takes off at a low altitude area, so the AGL is lowered when moving

to an object at a high altitude, and thus the area of the captured DW becomes very small. When the DW is small, there may be no overlap between captured images. Notably, this study failed to register images at the lowest flight altitude (50 m) and overlap (FL: 60%–70% SL: 30%–40%). However, Table 4 shows that when the overlap was high (FL: 80%–90% SL: 50%–60%), as in case B, images were registered and 3D spatial information could be obtained even at the lowest flight altitude. This indicates that when the difference in elevation is high compared with the flight altitude, image registration will not be possible when applying a low overlap; however, if high overlap is adopted while taking the photograph, registration will be possible despite the decrease in DW.

Based on the results above, it is worth considering that the starting point of an UAV should be set to a high altitude for a site with large variations in elevation; if this is not possible, there may be large differences in the flight case results. However, as long as the flight altitude and overlap can be set in a manner that will lead to a high accuracy, the flight will be efficient in terms of time and cost savings. Furthermore, if the relief of a subject photographed by the UAV is reflected so that the flight altitude can be modified in real time, the overlap can be maintained constantly. However, since the accuracy of 3D spatial information is essential, setting the flight

altitude and overlap in advance would produce the highest accuracy and optimize time and cost.

When the same flight altitude and number of GCPs were applied, the accuracy could be analyzed according to the overlap. Among the 49 cases, G-5 and H-5 are considered as examples. These two cases applied a flight altitude of 150 m and 20 GCPs. G-5 had overlaps of 60%–70% (FL) and 30%–40% (SL), while H-5 had overlaps of 80%–90% (FL) and 50%–60% (SL). The RMSE was 0.29 m in G-5 and 0.13 m in H-5. This confirmed that a higher overlap resulted in a higher accuracy, which is consistent with previous studies.

The accuracy of the 3D spatial information needs to be discussed according to the number of GCPs as well as flight parameters (flight altitude and overlap). Agüera-Vega et al. (2017) and Coveney and Roberts (2017) argued that there were no differences in the RMSEs derived from 15 GCPs. This study showed a similar result. As shown in Figure 9, when the flight altitude was 100 m or lower (cases A–D), differences in accuracy were not significant when 15 or 20 GCPs were used. When the flight altitude was 100 m or more (cases E–H), there was not a large difference in the accuracy among different GCPs numbers.

The number of GCPs needs to be considered in relation to the area of a

study site. Coveney and Roberts (2017) showed that accuracy was high when one GCP was used per 2 ha. In Agüera-Vega et al. (2017), the area of the site was 17.64 ha and there was no significant variation when the number of GCPs changed to around 15. Accordingly, one GCP was needed every 1.17 ha. This study required two GCPs per ha when the flight altitude of the UAV exceeded 100 m. However, when the UAV flew below 100 m, three GCPs were necessary per ha. Consequently, more GCPs are needed in areas with large variations in elevation and to increase accuracy during flight at lower altitudes.

In the present study, the camera calibration parameters were derived for each case using self-camera calibration. Follow-up studies should directly calibrate cameras using GCP or chess board indoor in various cases and compare the results with the self-camera calibrated values. As a result of examining the influence of the gimbal for each case, the higher the altitude and the overlapping ratio, the smaller the standard deviations of pitch and roll. The study areas included areas showing significant differences in altitude. Unlike previous studies, in this study, the accuracy of the 3D spatial information was high in areas at high flight altitude. Similarly, the higher the flight altitude, the lower the standard deviations of pitch and roll, which needs to be further elaborated in follow-up studies.

1.3. Computation of the Amount of Waste and Optimal flights parameters

The waste quantity for the 3D spatial data generated for all 49 cases constructed based on flight parameters and the number of GCPs was calculated and arranged according to the *xyz* (3D) RMSE accuracy. The overall flow from the photographing of the waste area to the estimation of the waste quantity is shown in Figure 25.

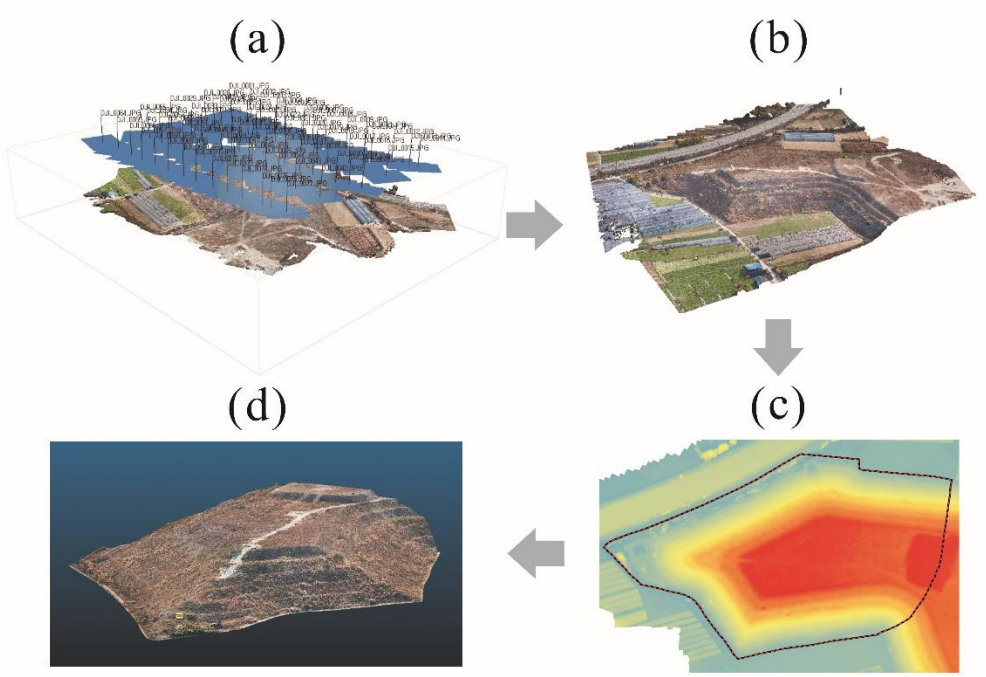

Figure 25 Waste quantity computation process : (a) UAV flight, (b) Point Clouds, (c) DSM, and (d) Volume computation

Since volume was calculated based on x, y, and z positions, it was judged that position accuracy had a direct impact on volume estimation. Numerous cases were established and the accuracy of 3D spatial information was compared with the volume computation results of each case. Previous studies have also regarded the position accuracy of the x, y, and z values as the accuracy of the results of volume computation (Yilmaz 2010; Hugenholtz et al. 2015; Rhodes 2017). However, they usually used 3D spatial information constructed using one flight case. In this study, 3D spatial data was compared with volume computation results obtained through 49 cases with numerous flight parameter settings. The results confirm that groups with a high position accuracy exhibit similar values for waste volume, while groups with low position accuracy have different values for the same. This indicates that the position accuracy of 3D spatial information has a direct impact on volume computation.

Volume estimation is mainly used in the field of Civil Engineering, which is incorporated by utilizing GPS or TLS. Recently, there are studies that use UAS in measuring the cut and fill of soil mass for excavation or embankment (Siebert and Teizer 2014; Akgul et al., 2018). The generation and analysis of DEMs are very important for civil engineering, and the costs are varied according to their accuracy and resolution (Akgul et al., 2018).

Figure 26 shows the DEM-based analysis of cuts and fills using UAV and GNSS in the civil engineering field. As the calculation of accurate cut and fill volume have a crucial impact on cost and time in civil engineering, accurate DEM generation is more important than time.

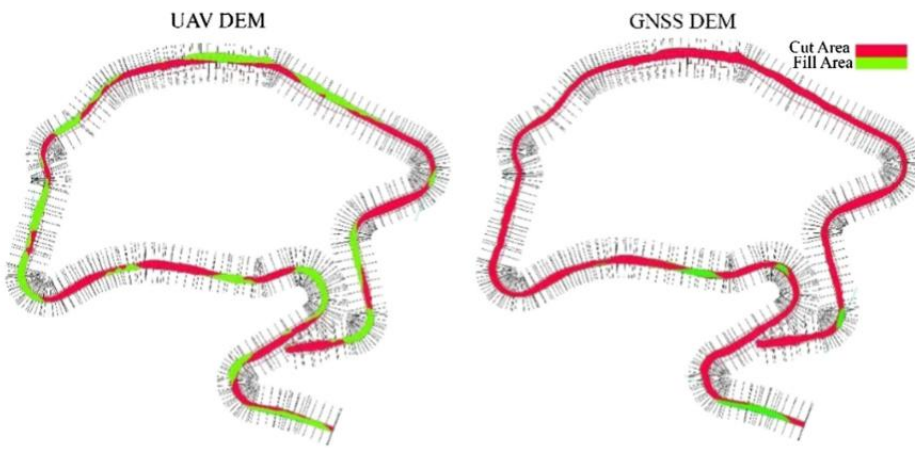

Figure 26 Cross sections and cut and fill areas using UAV- and GNSS-based DEM (Akgul et al., 2018)

However, difference in waste quantity estimation can be discussed in terms of time. While the accurate volume of waste quantity for responding to a large-scale disaster should be estimated within a short amount of time, accuracy must be prioritized for estimating earthwork volume.

Flight case D-7 had the highest accuracy, with an *xyz* (3D) RMSE of

about 0.08 m. Case G-1 had the lowest accuracy, with an *xyz* (3D) RMSE of about 124.75 m. The point cloud constructed via the two cases is shown in Figure 27 To the extent that a large number of point clouds are generated, differences in accuracy are not easy to distinguish in terms of relevance.

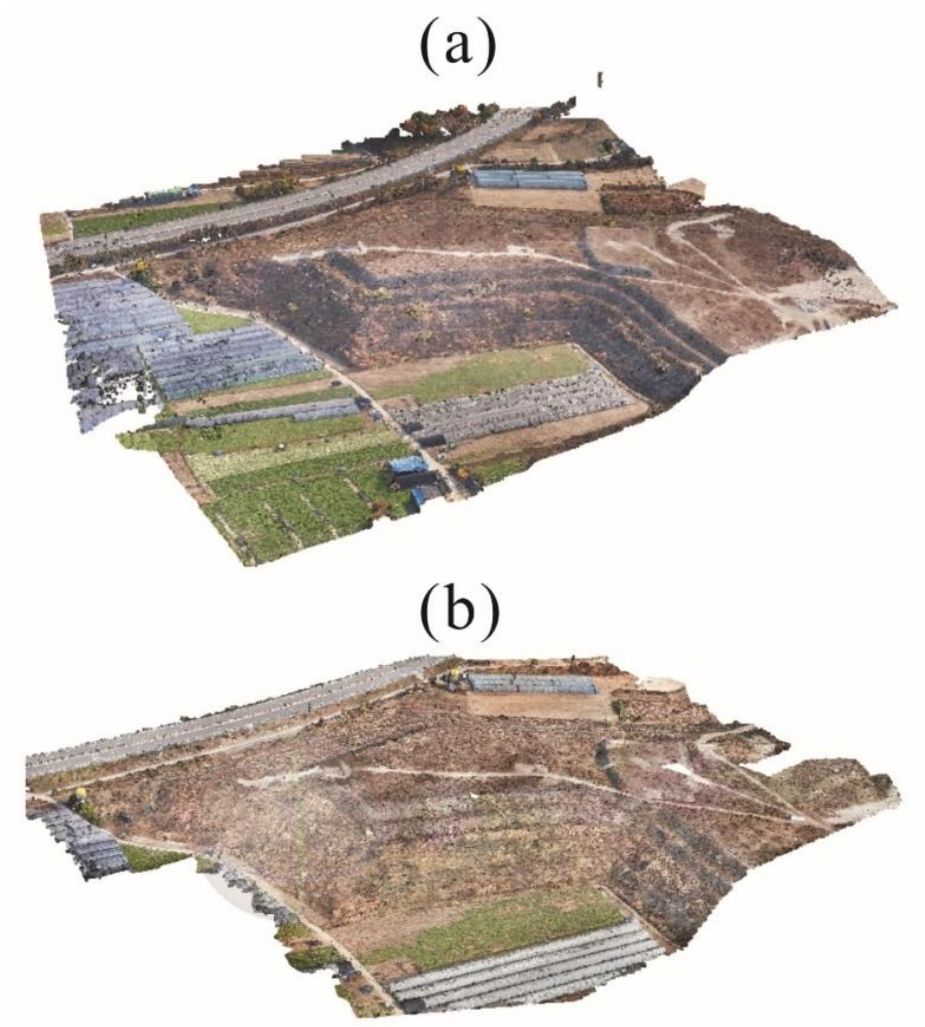

Figure 27 Point Clouds : (a) Case D-7 (High Accuracy), (b) Case G-1 (Low Accuracy)

However, if a DSM is created through two cases which have a large difference in accuracy, it is possible to confirm parts of the low-accuracy G-1 case that are not created properly in the DSM of the low-accuracy G-1 case (Fig. 28).

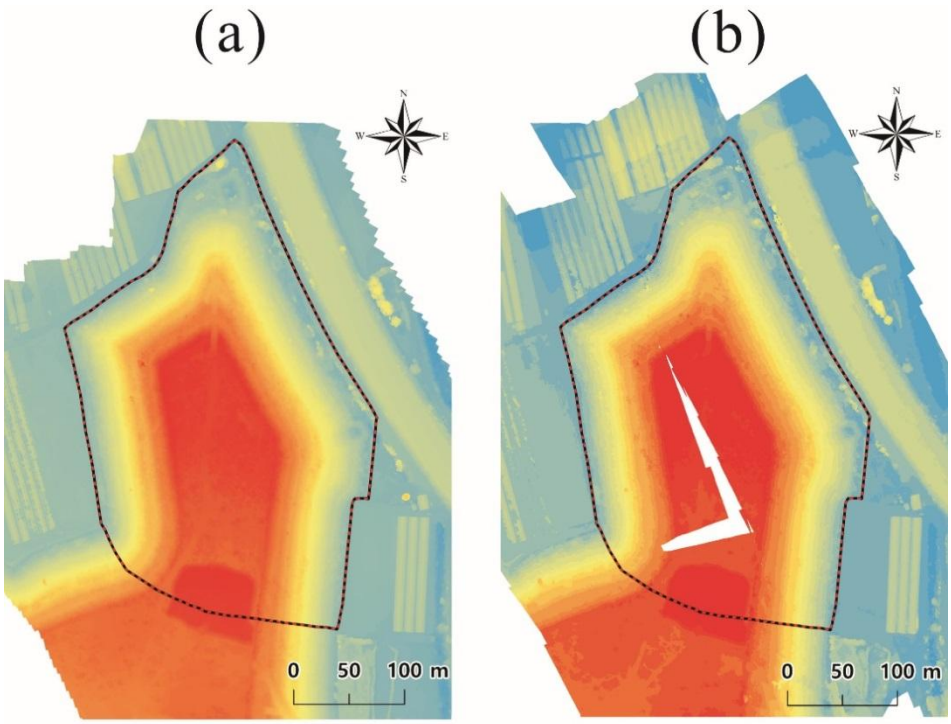

Figure 28 DSM : (a) Case D-7 (High Accuracy), (b) Case G-1 (Low Accuracy)

The waste quantity calculated ranged from 69,000 to 96,000 m^3. The top 10 cases in terms of accuracy had *xyz* (3D) RMSEs below 0.20 m, and the amount of waste was about 770,000 m^3 in each case, i.e., there were no large variations detected in terms of the amount of waste. However, the

lowest 10 cases in terms of accuracy had *xyz* (3D) RMSEs over 1 m; when no GCP was applied, the RMSE exceeded 100 m. The amount of waste in those 10 cases ranged from 693,382.7 to 961,223.7 m^3, and the estimates showed very large variations compared with the top 10 cases. In other words, when 3D spatial information sets were highly accurate in terms of location, they showed a similar tendency for waste amount. For the other 3D spatial information sets with low location accuracies, the estimated waste amounts displayed large differences.

Among 49 cases, top 15 cases that have the highest accuracy were derived along with elapsed time (Table 9).

Table 9 Time spent building 3D spatial information with the top 15 highest accuracy

Case	*xyz* (RMSE [m])	Entire of work time(minute)	Flight altitude(m) and Overlap*, / Flight time(minute)		Number of GCP survey time(minute)		Number of CPs survey time(minute)	Image processing time (minute)
D-7	0.08	954.87	80, ↑	20	30	60	109 30	847.87
D-6	0.10	941.82	80, ↑	20	25	50		871.82
F-6	0.11	442.5	120, ↑	9	25	50		383.50
D-5	0.11	924.77	80, ↑	20	20	40		864.77
F-7	0.13	451.45	120, ↑	9	30	60		382.45
H-5	0.13	131.15	150, ↑	4	20	40		87.15
H-4	0.14	121.17	150, ↑	4	15	30		87.17
F-4	0.14	420.47	120, ↑	9	15	30		381.47
H-3	0.14	111.12	150, ↑	4	10	20		87.12
G-7	0.15	98.27	150, ↓	3	30	60		35.27

F-5	0.15	430.38	120, ↑	9	20	40		381.38
D-4	0.15	923.82	80,↑	20	15	30		873.82
F-3	0.16	409.35	120, ↑	9	10	20		380.35
B-6	0.16	1051.65	50, ↑	46	25	50		955.65
B-5	0.17	1058.78	50, ↑	46	20	60		952.78
		* ↑ : Forward lap 80-90%, Side lap 50-60% ↓ : Forward lap 60-70%, Side lap 30-40%						

In the event of a disaster or when a decision about waste treatment needs to be made quickly, sufficient time should be given for estimating the amount of waste using an UAS. Among the top 15 cases, H-3, H-4, and H-5 had flight times of 4 min, and even if the time to measure the GCPs or analyze the 86 images is included, the results were obtained in a very short time. Case D-7 constructed very accurate 3D spatial information; however, the flight time was 20 min and 30 GCPs were measured and it took a very long time to analyze the 500 images. Thus, D-7 is inappropriate for estimating waste generation within a short time (e.g., during disaster situations where time is a factor). If a quick and accurate estimate of waste is needed at a site with large variations in elevation, a relatively high overlap should to be set, even at a high flight altitude, and about 15 GCPs need to be reflected to build appropriate 3D spatial information. When the SfM technique is used, internal orientation, such as camera calibration, needs to be performed in advance in addition to the measurement of the GCPs.

Conventional methods of calculating waste generation can be compared in terms of accuracy and speed. When the basic unit of material or the modeling approach is used to estimate waste generation, data obtained before the latter is applied, and various parameters influencing waste generation, cannot be considered. For this reason, estimates are often different from the levels of real waste generation. Relatively recent technological developments have enabled GPS or TLS techniques to be used to estimate waste, and such data can achieve considerable accuracy. However, these methods are not always practical because of speed or cost issues.

2. Comparison and Analysis of TLS and UAS-based 3D Spatial Information

2.1. Generation of 3D Spatial Information and Volume Computation using UAS

The TLS-based point cloud data were obtained by scanning the survey area from all 20 scan positions. The individual scan data were registered into a single point cloud, and a fairly high accuracy was obtained (RMSE = 0.202 m). The volume computed using the TLS-based point cloud was 41,226 m^3. Figure 29 is TLS-based point cloud and DSM.

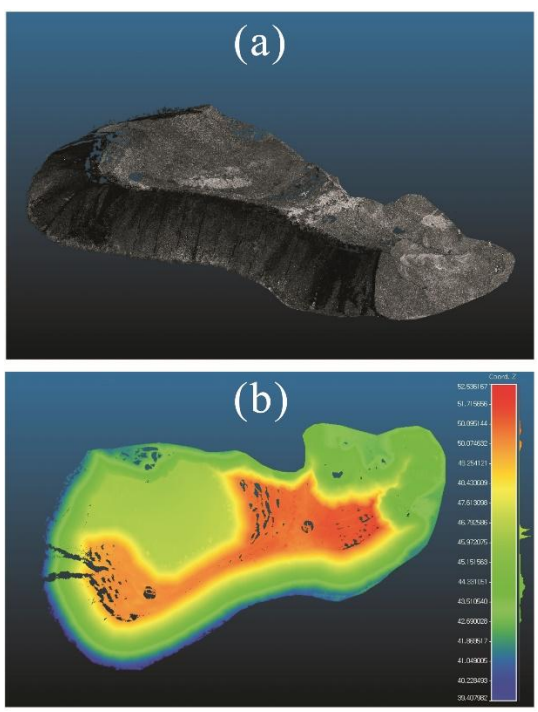

Figure 29 TLS-based 3D spatial information (a) Point clouds, (b) DSM

UAS-based point clouds were generated according to a total of eight cases (A–H), with four flight altitudes and two sets of 10 GCPs as variables.

Table 10 UAS-based point cloud accuracy depending on UAV flight cases

Flight Altitude (m)	Overlap (FL: 85%/SL: 65%)					
	10 GCPs (considering waste height)			10 GCPs (without considering waste height)		
	Case	*xyz* RMSE (m)	Number of images	Case	*xyz* RMSE (m)	Number of images
40	A	0.032	443	B	0.447	443
80	C	0.055	133	D	0.293	133
120	E	0.075	65	F	0.325	65
160	G	0.104	23	H	0.193	23

Among the eight cases in which point clouds were generated, Case A was found to be the most accurate (RMSE = 0.032 m). Figure 30 is UAS-based point cloud and DSM of Case A.

Case A was configured with a flight altitude of 40 m and a set of 10 GCPs considering waste height. In the cases considering waste height (A, C, E, and G), the RMSE increases with increasing flight altitude, which means that the accuracy is inversely correlated with the flight altitude. In the cases with evenly distributed GCPs (B, D, F, and H) without considering waste height, no correlation was observed between the RMSE and flight altitude.

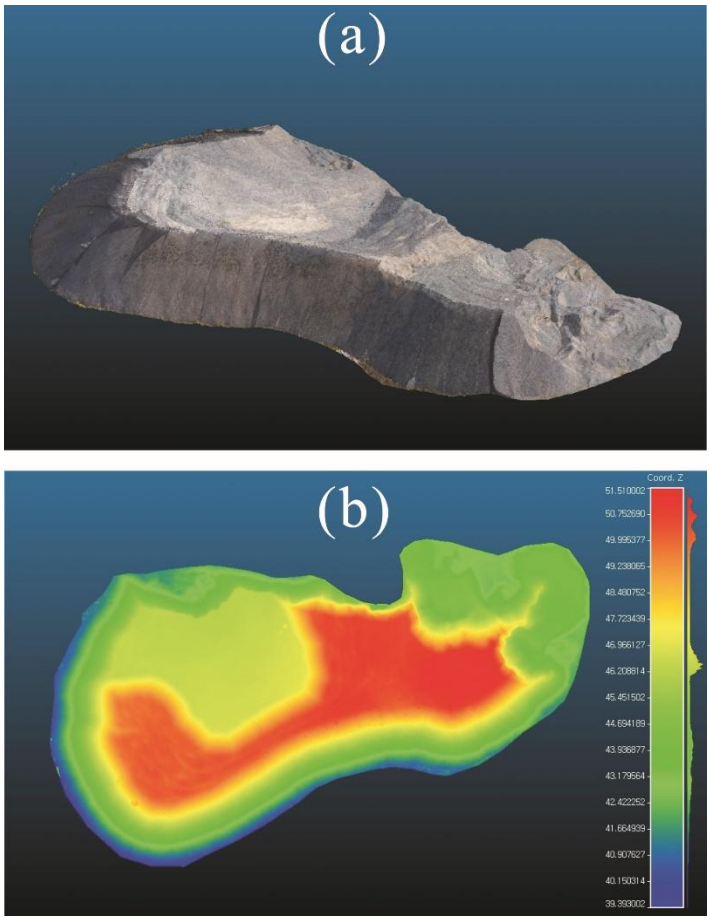

Figure 30 UAS-based 3D spatial information: (a) Point clouds, (b) DSM

In general, at a lower flight height, the image resolution is enhanced and more images are taken, with more overlapping parts, resulting in higher image quality and accuracy. However, no significant effect of flight altitude was observed when the GCPs were placed only on flat land. This finding suggests that the GCP arrangement is associated with the accuracy of the point cloud model. Previous studies have mostly been focused on the

number of GCPs, rather than on their placement, and they were conducted in areas with only slight elevation variations. The results of this study demonstrate that GCPs should also be placed at the highest points in an area with significant elevation variations.

Although the UAS method outperformed the TLS approach in terms of point cloud accuracy, this finding does not necessary mean that UAS technology is superior to TLS technology. In the UAS approach, an optimized point cloud could be built by selecting the best performing case among eight different cases. If the TLS method had been conducted using a similar experimental setup, i.e., with more scan stations and more elaborate measurements, its accuracy would have been higher. Jo and Hong (2019) built point clouds of the same target object using TLS and UAS technologies and computed the accuracies of the x, y, and z coordinates, finding that that the TLS approach yielded more accurate x and y coordinates, while the UAS method generated slightly more accurate z coordinates. There remains considerable room for discussion regarding the performances of these two techniques in terms of other factors as well, such as time, cost, and efficiency.

Volume computation was conducted on the eight UAV flight cases using the corresponding point clouds (Table 11).

Table 11 Volume computation by UAV flight case

Case	Volume (m^3)	Case	Volume (m^3)
A	41,256	B	43,042
C	41,405	D	42,818
E	41,449	F	43,013
G	41,621	H	42,578

Among the eight cases (A–H), in which volume computation was performed, those with GCPs placed atop the waste pile (A, C, E, and G) exhibited similar values (~41,000 m^3). This finding may be examined in association with the RMSE. Cases A, C, E, and G, which demonstrated high point cloud accuracy, yielded similar volumes, while in the other cases (B, D, F, and H), the computed volumes deviated considerably from one another. Thus, it can be concluded that the point cloud accuracy directly influences the volume computation accuracy.

2.2. Spatial Comparison and Analysis

The M3C2 algorithm was employed to compare and analyze the point clouds generated using TLS and UAS technologies. For the UAS-based point cloud, Case A, which had the highest accuracy, was used. Whereas both the TLS and UAS methods yielded point clouds with fairly high

accuracies, their respective drawbacks were observed.

Figs. 31 (a) and (b) show side-view images comparing the TLS- and UAS-based point clouds of the waste disposal site.

Figure 31 (a)-1 and (b)-1 depict the point clouds generated using the TLS approach, and Figure 31(a)-2 and (b)-2 present those obtained using the UAS method. The latter two images show missing portions, presumably due to the difference between the TLS position and UAV shooting position. TLS technology scans sideways from positions fixed on the ground, but UAV images taken from above are more likely to miss side-view aspects. It is of course possible to construct a model close to the original shape, using SfM algorithms, with images taken from different positions as configured when setting the UAV flight parameters. However, this technique was not sufficiently elaborate to reproduce the irregular curved sides.

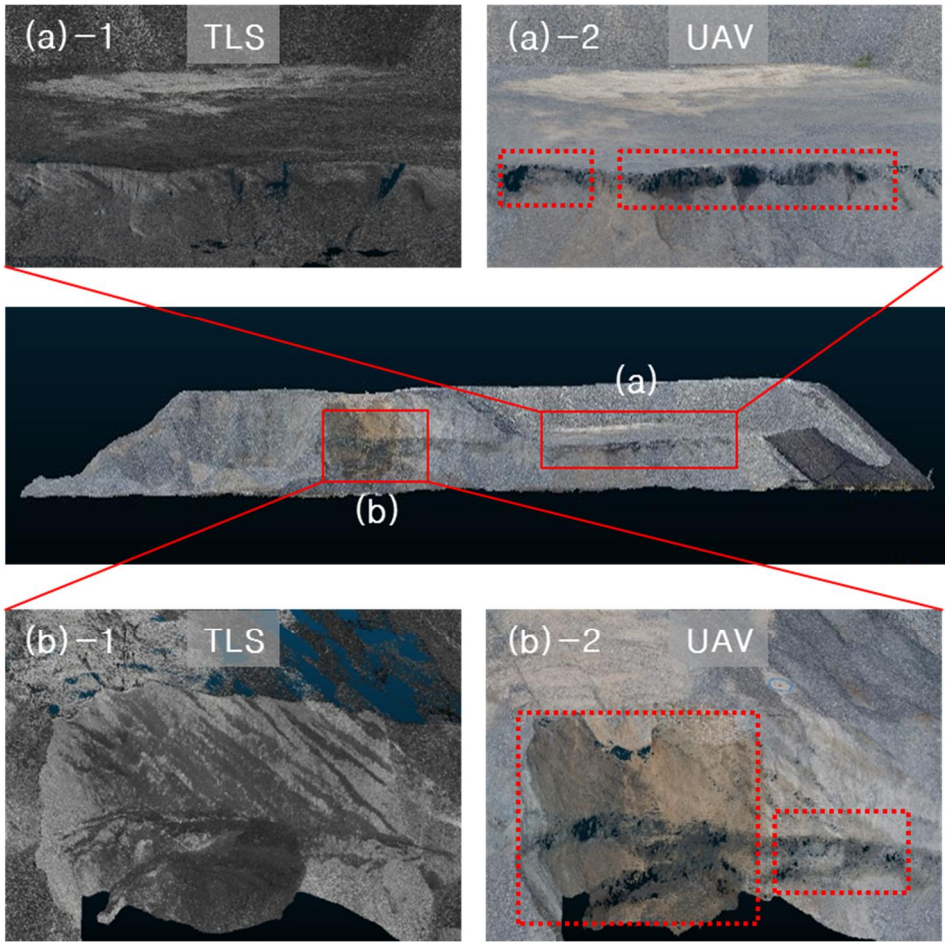

Figure 31 Side-view point clouds of the waste disposal site: (a)-1 TLS-based point cloud, (a)-2 UAS-based point cloud; (b)-1 TLS-based point cloud, (b)-2 UAS-based point cloud

Figure 31 (a) and (b) show top-view images comparing the TLS- and UAS-based point clouds of the waste disposal site.

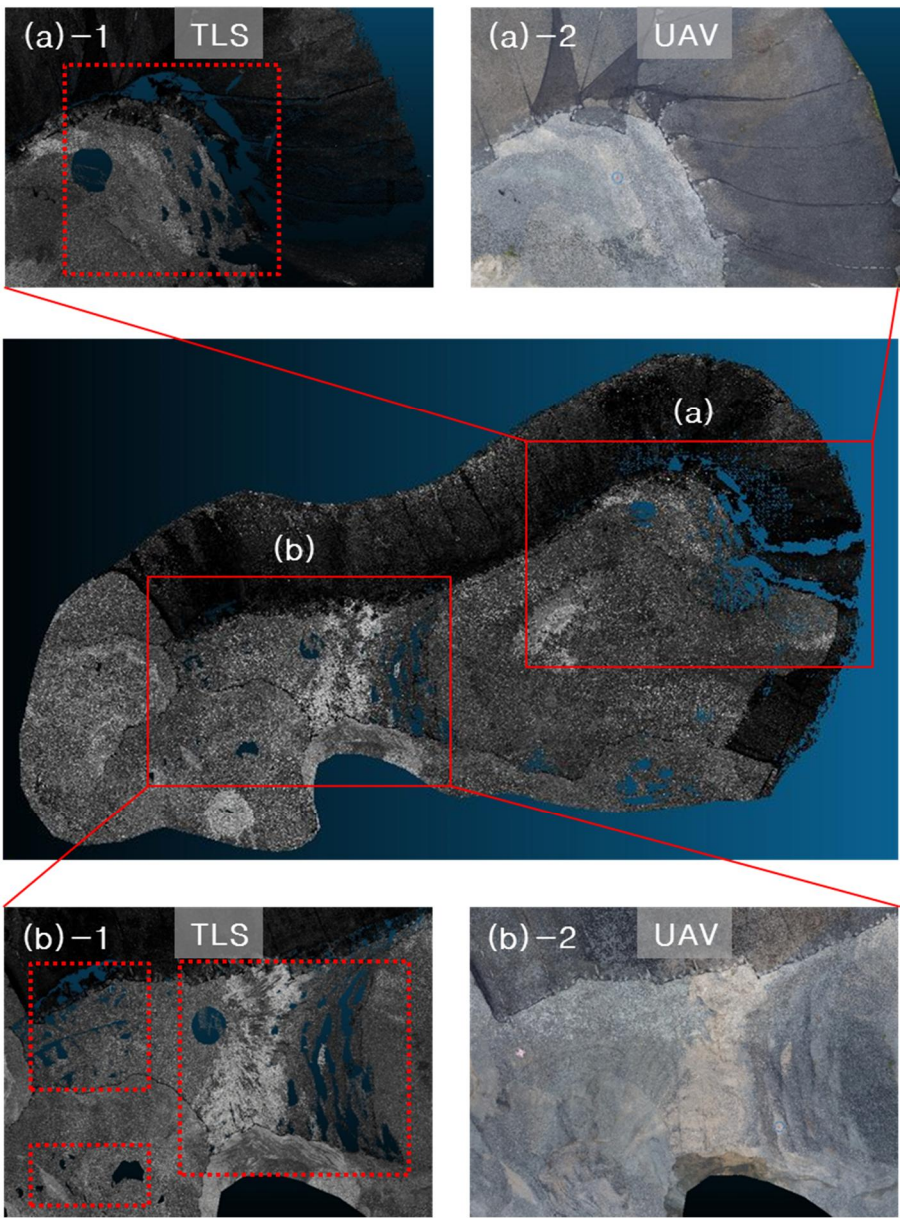

Figure 32 Top view of the waste point cloud: (a)-1 TLS-based point cloud; (a)-2 UAV-based point cloud; (b)-1 TLS-based point cloud; (b)-2 UAV-based point cloud

Figure 32 (a)-1 and (b)-1 are images of the TLS-based point cloud, and Figure 32 (a)-2 and (b)-2 depict the UAS-based point cloud. Here, the TLS-based point cloud exhibits unskinned portions, although TLS was also performed on the top of the waste pile, presumably due to the uneven surface with steps and grooves. The TLS method was found to be particularly prone to errors in representing grooves in the point cloud. In contrast, the grooves and curves are well reflected in the UAS-based point cloud. In addition to the advantage of the vertical shooting position of a UAV in taking top-view photos, as mentioned in the discussion of the side-view images, the GCPs placed atop the waste pile presumably contributed to the representation accuracy.

3. Multispace Fusion Methodology-based 3D Spatial Information Generating and Efficiency Analysis

3.1. Multispace Fusion Methodology-based 3D Spatial Information

Single point cloud was built by fusing the TLS- and UAS-based point clouds. Figure 33 is TLS/UAS-based point cloud and DSM.

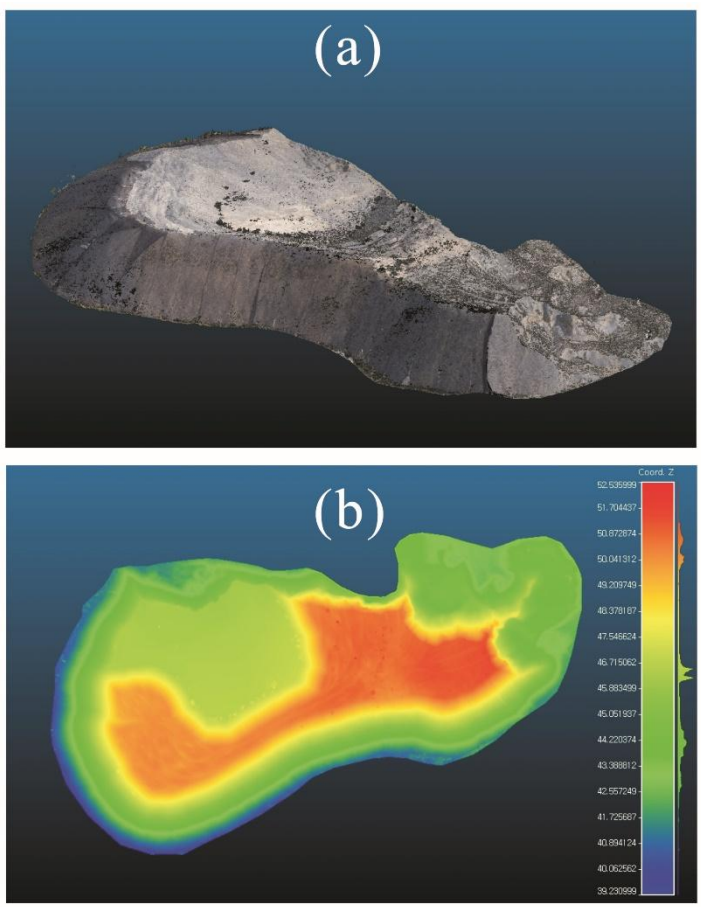

Figure 33 Fusion method-based Point cloud: (a) Point clouds, (b) DSM

The fusion model yielded the following values: RMSE = 0.030 m and volume = 41,232 m^3 (Table 12).

Table 12 Point cloud accuracy and volume computation results of the UAV, TLS, and TLS/UAV fusion models

	UAS	TLS	Fusion
xyz RMSE (m)	0.032	0.202	0.030
Volume (m^3)	41,256	41,226	41,232

The point cloud accuracy of the fusion model was higher than those of the TLS and UAS methods, but very similar to that of the UAS method. Müller et al. (2017) constructed a high-resolution DEM by fusing the TLS and UAS technologies to monitor an eruption site. Although a fusion model was used to reflect the geomorphological characteristics of the study area, the comparison and analysis results revealed that the UAS approach alone could yield the desired results.

In the TLS/UAS point cloud fusion model, TLS and UAS technology can of course mutually compensate for the drawbacks of the other. TLS is advantageous over UAS technology when surveying a small area in terms of image accuracy but has limitations in surveying large areas (Chen et al., 2015). Jo and Hong (2019) suggested that in the fusion of UAS- and TLS-

based point clouds of an area with buildings and surrounding grounds, a UAS can be employed to obtain the point cloud at the top of the building, which is difficult to obtain via TLS, thereby enhancing the overall accuracy of the 3D point cloud data.

In this study, TLS and UAS methods were applied to the sides and top of the waste pile, respectively, and found that such integrated use of TLS and UAS technologies can compensate for the drawbacks of each. However, given the insignificant difference in accuracy between the UAS- and fusion model-based point clouds, the efficacies of these methods must be examined further. The total time spent on point cloud generation was 800 min for TLS and 340 min for the UAS. The fusion model required considerably more time because of its own analysis time in addition to the time taken for the TLS and UAS approaches. Consequently, the UAS method may be considered highly advantageous from the viewpoint of efficiency.

In summary, the fusion model may be a rational solution to the problems of UAS and TLS technologies, but has lower efficiency than the UAS approach. The UAS method was found to be prone to error in side-view photogrammetry in point cloud generation, but this problem can be overcome by UAS tilt control and flying along the sides of a waste pile. The insufficient representation of the sides in the point cloud obtained in this

study is ascribable to the limitation of the vertical UAS shooting position. In view of this insufficiency, future research must be conducted that focuses on deriving an optimal configuration of various flight parameters, such as the camera position and direction, to enhance the accuracy of point cloud generation and volume computation.

3.2. 3D Spatial information Efficiency Analysis for Responding to Large-scale Disasters

In chapter 1, cross correlation between four major variables (GCPs survey time, Flight time, Image processing time, and *xyz* RMSE that is the accuracy of 3D spatial information) was analyzed through Pearson correlation analysis (Table 13). The correlation between flight time and processing time was significantly positive ($p<0.01$, $r=0.888$), and the positive correlation between GCPs survey time and *xyz* RMSE was verified ($p<0.01$, $r=0.511$).

Table 13 Time and accuracy of 3D spatial information construction Correlation analysis between variables

		GCPs survey time	Flight time	Image processing time	xyz RMSE
GCPs survey time	Pearson Correlation	1	.000	.005	.551"
	Sig. (2-tailed)		1.000	.976	.001
	N	42	42	42	42

Flight time	Pearson Correlation	.000	1	.888"	.062
	Sig. (2-tailed)	1.000		.000	.698
	N	42	42	42	42
Image processing time	Pearson Correlation	.005	.888"	1	.364'
	Sig. (2-tailed)	.976	.000		.018
	N	42	42	42	42
xyz RMSE	Pearson Correlation	.511"	.062	.364'	1
	Sig. (2-tailed)	.001	.698	.018	
	N	42	42	42	42

**. Correlation is significant at the 0.01 level (2-tailed)
*. Correlation is significant at the 0.05 level (2-tailed)

Long flight time is due to taking multiple images while flying at low altitude with high redundancy. In this case, more images are captured than when the images are taken at high altitude with low redundancy. It affects image processing time. Therefore, there is a high chance that it resulted in the significantly positive correlation between flight time and processing time.

The time was calculated required to generate a point cloud, i.e., from the beginning of TLS and UAV flight to point cloud completion, to compare the time requirements of TLS and UAS technologies (Table 14).

Table 14 Time requirements for TLS- and UAV-based point cloud generation

Point cloud	Scan/flight time	GCPs measurement	CPs measurement	Image processing	Total
TLS	120 min	20 min	50 min	610 min	800 min
UAS	20 min	50 min	50 min	220 min	340 min

The TLS and UAS methods required 800 and 340 min, respectively. The same amount of time was spent measuring CPs, which were used for accuracy evaluation, because the same data were used for the TLS and UAS tests. Except for the time for measuring the GCPs, TLS required more time. Given the small size of the waste in the study area compared with large disaster waste, the feasibility of TLS technology for volume computation is considered low.

A comparison was made of the costs spent to construct point clouds using the two technologies (Table 15).

Table 15 Costs requirements for TLS-and UAS based point cloud generation

Equipment	Costs of survey equipment	Costs of labor per day (Engineer Cadastral Surveying)	Costs of software	Total
TLS (Leica P40)	$102,000 USD	$210 USD	Cyclone 9.2.1 ($8,340 USD)	$110.550 USD
UAV (DJI Inspire 1 pro)	$4,000 USD	$210 USD	Pix4d mapper 4.3 ($4,990 USD)	$9,200 USD

The TLS cost was high compared to the UAV, and each technology's expert cost was found to be the same at the daily level. In regards to the software cost needed for data analysis, the TLS had a high cost, and overall the cost spent on TLS was higher than that on UAS. In terms of the three

previously analyzed factors of accuracy, time spent, and cost, it can be confirmed that UAS is superior in all areas. As mentioned earlier, UAS technology cannot be declared superior to TLS technology due to these factors. This is because the TLS measurement method's accuracy can be increased further through elaboration. However, in terms of cost and time, UAS can be considered more efficient regardless of what methodology is used.

In large-scale disaster cases, it is necessary to give priority to time and accuracy and select feasible technologies. This is because during a large-scale disaster, waste must be handled quickly and efficiently in a short time. This being the case, waste material calculations which use UAS technology can be considered advantageous in a large-scale disaster.

IV. Conclusion

This study used UAS to build a 3D spatial information and examined its feasibility for waste quantity calculations. Also, TLS technology, which has been used to build 3D spatial information in the past, was used to perform analysis and comparisons with the UAS technology. Finally, the 3D spatial information based on the two technologies were combined, and accuracy and efficiency were analyzed.

A UAS-based 3D spatial information was built, and it was discovered that the results were contrary to previous studies due to the DW (Distance covered on the ground by on image in Width direction) in waste regions with a lot of altitude differences. Normally, as the altitude becomes lower, the accuracy of the 3D spatial information becomes higher, but in this study it was found that the accuracy became lower as the altitude became lower. After the UAS-based 3D spatial information's waste calculation feasibility was confirmed, it was compared to the 3D spatial information that was based on the two technologies.

It was possible to examine the advantages and disadvantages of each 3D spatial information. As for accuracy, the RMSE of the UAS-based 3D spatial information was 0.032 m, and the RMSE of the TLS model was

0.202, making the UAS model's accuracy higher. The RMSE of the 3D spatial information which combined the two technologies was 0.030 m, and it showed the highest accuracy of the three methodologies.

UAV, which take aerial photographs vertically, are not able to capture the detailed side looks of an object. On the other hand, TLS is unable to capture the top of an object as it takes photographs on the ground. In the tests of generating the 3D spatial information of a waste pile using the two techniques, it was identified that point clouds were not created properly; for the unmanned aircraft system UAS-based 3D spatial information, the point cloud was not properly created for the sides, while for the TLS-based 3D spatial information, the point cloud was not properly created for the top. The choice between the two techniques may depend on actual situation or special needs.

Unlike the civil engineering field, the calculation of a waste pile volume requires efficiency in time, as well as accuracy as the basis. Accordingly, this study sought to discuss efficiency in terms of time and cost. Although the 3D spatial information with high accuracy was attainable by either TLS or UAS technique, the UAS-based 3D spatial information was more advantageous in both cost and time, requiring less cost and time. As waste piles generated from disasters should be taken out as quickly as possible, the

calculation of waste volumes using TLS is unlikely to be applied in disaster situations.

The major drawback of UAVs is that it they are extremely sensitive to weather conditions. Since UAV flight is impossible in inclement weather, countermeasures are required and the legal and policy systems restricting UAV flight also need to be reconsidered.

During large-scale disasters, it is necessary to respond in a relatively short time to minimize damage and perform a variety of decision-making. The UAS-based 3D spatial information building method found in this study can be used for large-scale waste amount calculations and spatial decision-making.

V. Bibliography

Aber, J. S., Marzolff, I., & Ries, J. (2010). Small-format aerial photography: Principles, techniques and geoscience applications. Elsevier.

Agüera-Vega, F., Carvajal-Ramírez, F., & Martínez-Carricondo, P. (2017). Assessment of photogrammetric mapping accuracy based on variation ground control points number using unmanned aerial vehicle. *Measurement*, *98*, 221-227.

Akgul, M., Yurtseven, H., Gulci, S., & Akay, A. E. (2018). Evaluation of UAV-and GNSS-Based DEMs for Earthwork Volume. *Arabian Journal for Science and Engineering*, *43*(4), 1893-1909.

American Red Cross (2015). Drones for Disaster Response and Relief Operations. American Red Cross.

Asari, M., Sakai, S. I., Yoshioka, T., Tojo, Y., Tasaki, T., Takigami, H., & Watanabe, K. (2013). Strategy for separation and treatment of disaster waste: a manual for earthquake and tsunami disaster waste management in Japan. *Journal of Material Cycles and Waste Management*, *15*(3), 290-299.

Barnhart, T., & Crosby, B. (2013). Comparing two methods of surface change detection on an evolving thermokarst using high-temporal-frequency terrestrial laser scanning, Selawik River, Alaska. *Remote Sensing*, *5*(6), 2813-2837.

Brown, C., Milke, M., & Seville, E. (2011). Disaster waste management: A review article. *Waste management*, *31*(6), 1085-1098.

Chen, J. R., Tsai, H. Y., Hsu, P. C., & Shen, C. C. (2007). Estimation of

waste generation from floods. *Waste management*, *27*(12), 1717-1724.

Chen, N., Ni, N., Kapp, P., Chen, J., Xiao, A., & Li, H. (2015). Structural analysis of the Hero Range in the Qaidam Basin, northwestern China, using integrated UAV, terrestrial LiDAR, Landsat 8, and 3-D seismic data. *IEEE Journal of Selected Topics in Applied Earth Observations and Remote Sensing*, *8*(9), 4581-4591.

Cignoni, P., Rocchini, C., & Scopigno, R. (1998, June). Metro: Measuring error on simplified surfaces. *In Computer Graphics Forum* (Vol. 17, No. 2, pp. 167-174). Oxford, UK and Boston, USA: Blackwell Publishers.

Cook, K. L. (2017). An evaluation of the effectiveness of low-cost UAVs and structure from motion for geomorphic change detection. *Geomorphology*, *278*, 195-208.

Côté, J. F., Fournier, R. A., & Egli, R. (2011). An architectural model of trees to estimate forest structural attributes using terrestrial LiDAR. *Environmental Modelling & Software*, *26*(6), 761-777.

Coveney, S., & Roberts, K. (2017). Lightweight UAV digital elevation models and orthoimagery for environmental applications: data accuracy evaluation and potential for river flood risk modelling. *International journal of remote sensing*, *38*(8-10), 3159-3180.

Coveney, S., Fotheringham, A. S., Charlton, M., & McCarthy, T. (2010). Dual-scale validation of a medium-resolution coastal DEM with terrestrial LiDAR DSM and GPS. *Computers & Geosciences*, *36*(4), 489-499.

Dietrich, J. T. (2016). Riverscape mapping with helicopter-based Structure-

from-Motion photogrammetry. *Geomorphology*, *252*, 144-157.

Dijkstra, J. J., van der Sloot, H. A., & Comans, R. N. (2002). Process identification and model development of contaminant transport in MSWI bottom ash. *Waste Management*, *22*(5), 531-541.

EPA. (2008). Planning for Natural Disaster Debris.

EPA. 2008. Planning for Natural Disaster Debris. U.S. Environmental Protection Agency.

Erdelj, M., & Natalizio, E. (2016, February). UAV-assisted disaster management: Applications and open issues. In *2016 international conference on computing, networking and communications (ICNC)* (pp. 1-5). IEEE.

Ezequiel, C. A. F., Cua, M., Libatique, N. C., Tangonan, G. L., Alampay, R., Labuguen, R. T., ... & Loreto, A. B. (2014, May). UAV aerial imaging applications for post-disaster assessment, environmental management and infrastructure development. In *2014 International Conference on Unmanned Aircraft Systems (ICUAS)* (pp. 274-283). IEEE.

FEMA. (2007). Public Assistance: Debris Monitoring Guide.

FEMA. (2010). Public Assistance: Debris Monitoring Guide.

Fonstad, M. A., Dietrich, J. T., Courville, B. C., Jensen, J. L., & Carbonneau, P. E. (2013). Topographic structure from motion: a new development in photogrammetric measurement. *Earth Surface Processes and Landforms*, *38*(4), 421-430.

Frolova, D., & Simakov, D. (2004). Matching with invariant features. *The*

Weizmann Institute of Science, March.

Gašparović, M., & Gajski, D. (2016, January). Two-step camera calibration method developed for micro UAV's. In *XXIII ISPRS Congress*.

Gašparović, M., & Jurjević, L. (2017). Gimbal influence on the stability of exterior orientation parameters of UAV acquired images. *Sensors*, *17*(2), 401.

Giannetti, F., Chirici, G., Gobakken, T., Næsset, E., Travaglini, D., & Puliti, S. (2018). A new approach with DTM-independent metrics for forest growing stock prediction using UAV photogrammetric data. *Remote Sensing of Environment*, *213*, 195-205.

Girardeau-Montaut, D., Roux, M., Marc, R., & Thibault, G. (2005). Change detection on points cloud data acquired with a ground laser scanner. *International Archives of Photogrammetry, Remote Sensing and Spatial Information Sciences*, *36*(part 3), W19.

Gonçalves, J. A., & Henriques, R. (2015). UAV photogrammetry for topographic monitoring of coastal areas. *ISPRS Journal of Photogrammetry and Remote Sensing*, *104*, 101-111.

Harwin, S., & Lucieer, A. (2012). Assessing the accuracy of georeferenced point clouds produced via multi-view stereopsis from unmanned aerial vehicle (UAV) imagery. *Remote Sensing*, *4*(6), 1573-1599.

Hu, Z. H., & Sheu, J. B. (2013). Post-disaster debris reverse logistics management under psychological cost minimization. *Transportation Research Part B: Methodological*, *55*, 118-141.

Hugenholtz, C. H., Walker, J., Brown, O., & Myshak, S. (2014). Earthwork

volumetrics with an unmanned aerial vehicle and softcopy photogrammetry. *Journal of Surveying Engineering*, *141*(1), 06014003.

Hugenholtz, C. H., Walker, J., Brown, O., & Myshak, S. (2014). Earthwork volumetrics with an unmanned aerial vehicle and softcopy photogrammetry. *Journal of Surveying Engineering*, *141*(1), 06014003.

James, M. R., Robson, S., & Smith, M. W. (2017). 3D uncertainty based topographic change detection with structure-from-motion photogrammetry: precision maps for ground control and directly georeferenced surveys. *Earth Surface Processes and Landforms*, *42*(12), 1769-1788.

Jeong, S. (2011). Evaluation of long-term stability of interior orientation parameters of a non-metric camera. *Journal of the Korean Society of Surveying, Geodesy, Photogrammetry and Cartography*, *29*(3), 283-291.

Jo, J. H., Kim, T. H., Yi, S. R., Lee, J. E., Kim, T. H., & Jeong, S. H. (2016). *Optimal Management of Disaster Waste by its Properties Using GIS.* Korea Environment Institute.

Jo, Y. H., & Hong, S. (2019). Three-Dimensional Digital Documentation of Cultural Heritage Site Based on the Convergence of Terrestrial Laser Scanning and Unmanned Aerial Vehicle Photogrammetry. *ISPRS International Journal of Geo-Information*, *8*(2), 53.

Kakooei, M., & Baleghi, Y. (2017). Fusion of satellite, aircraft, and UAV data for automatic disaster damage assessment. *International journal of remote sensing*, *38*(8-10), 2511-2534.

Kalacska, M., Chmura, G. L., Lucanus, O., Bérubé, D., & Arroyo-Mora, J. P. (2017). Structure from motion will revolutionize analyses of tidal wetland landscapes. *Remote Sensing of Environment*, *199*, 14-24.

Kim, W. I., Kang, Y. R., Kim, N., Jo. Y. A., Yeon, J. M., Jeong. S. K., Kim, M. S., Yoon, C. W., Shin, S. K., & Oh K. J. (2012). *Japan Disaster Waste Sorcebook*. National Institute of Envoronmental Research.

Lague, D., Brodu, N., & Leroux, J. (2013). Accurate 3D comparison of complex topography with terrestrial laser scanner: Application to the Rangitikei canyon (NZ). *ISPRS journal of photogrammetry and remote sensing*, *82*, 10-26.

Lee, Y. C. (2015). Assessing the positioning accuracy of high density point clouds produced from rotary wing quadrocopter unmanned aerial system based imagery. *Journal of Korean Society for Geospatial Information System*, *23*(2), 39-48.

Lowe, D. G. (2004). Distinctive image features from scale-invariant keypoints. *International journal of computer vision*, *60*(2), 91-110.

Mancini, F., Dubbini, M., Gattelli, M., Stecchi, F., Fabbri, S., & Gabbianelli, G. (2013). Using unmanned aerial vehicles (UAV) for high-resolution reconstruction of topography: The structure from motion approach on coastal environments. *Remote Sensing*, *5*(12), 6880-6898.

McLoughlin, D. (1985). A framework for integrated emergency management. *Public administration review, 45*, 165-172.

Mesas-Carrascosa, F. J., Notario García, M., Meroño de Larriva, J., & García-Ferrer, A. (2016). An analysis of the influence of flight

parameters in the generation of unmanned aerial vehicle (UAV) orthomosaicks to survey archaeological areas. *Sensors*, *16*(11), 1838.

Mesas-Carrascosa, F. J., Torres-Sánchez, J., Clavero-Rumbao, I., García-Ferrer, A., Peña, J. M., Borra-Serrano, I., & López-Granados, F. (2015). Assessing optimal flight parameters for generating accurate multispectral orthomosaicks by UAV to support site-specific crop management. *Remote Sensing*, *7*(10), 12793-12814.

Müller, D., Walter, T. R., Schöpa, A., Witt, T., Steinke, B., Gudmundsson, M. T., & Dürig, T. (2017). High-resolution digital elevation modeling from TLS and UAV campaign reveals structural complexity at the 2014/2015 Holuhraun eruption site, Iceland. *Frontiers in Earth Science*, *5*, 59.

Pérez, M., Agüera, F., & Carvajal, F. (2013). Low cost surveying using an unmanned aerial vehicle. *Int. Arch. Photogramm. Remote Sens. Spat. Inf. Sci*, *40*, 311-315.

Petak, W. J. (1985). Emergency management: A challenge for public administration. *Public Administration Review*, *45*, 3-7.

Pineux, N., Lisein, J., Swerts, G., Bielders, C. L., Lejeune, P., Colinet, G., & Degré, A. (2017). Can DEM time series produced by UAV be used to quantify diffuse erosion in an agricultural watershed?. *Geomorphology*, *280*, 122-136.

Raeva, P. L., Filipova, S. L., & Filipov, D. G. (2016). VOLUME COMPUTATION OF A STOCKPILE-A STUDY CASE COMPARING GPS AND UAV MEASUREMENTS IN AN OPEN PIT QUARRY. *International Archives of the Photogrammetry, Remote*

Sensing & Spatial Information Sciences, *41*.

Reinhart, D. R., & Mccreanor, P. T. (1999). Disaster debris management–planning tools.

Restas, A. (2015). Drone applications for supporting disaster management. *World Journal of Engineering and Technology*, *3*(03), 316.

Rhodes, R. K. (2017). UAS as an Inventory Tool: A Photogrammetric Approach to Volume Estimation.

Siebert, S., & Teizer, J. (2014). Mobile 3D mapping for surveying earthwork projects using an Unmanned Aerial Vehicle (UAV) system. *Automation in construction*, *41*, 1-14.

Silva, C. A. D., Duarte, C. R., Souto, M. V. S., Santos, A. L. S. D., Amaro, V. E., Bicho, C. P., & Sabadia, J. A. B. (2016). Evaluating the accuracy in volume calculation in a pile of waste using UAV, GNSS and LiDAR. *Boletim de Ciências Geodésicas*, *22*(1), 73-94.

Smith, M. W., Carrivick, J. L., & Quincey, D. J. (2016). Structure from motion photogrammetry in physical geography. *Progress in Physical Geography*, *40*(2), 247-275.

Son, S. W., Yoon, J. H., Jo, J. H., Kim, T. H., Jeon, H. J. (2016). *Analysis of Disaster Response Technologies that Use Drones and Trend of Research*. Korea Environmental Institute.

Son, S. W., Yu J.J., Jeon, H.J., Lim, S.H., Kang, Y.E., & Yoon, J.H. (2017). Investigation of Measurement Feasibility of Large-size Wastes Based on Unmanned Aerial System. *Korean Journal of Remote Sensing, 33*(5-

3), 809-820.

Srinivas, H., & Nakagawa, Y. (2008). Environmental implications for disaster preparedness: Lessons Learnt from the Indian Ocean Tsunami. *Journal of environmental management*, *89*(1), 4-13.

Udin, W. S., & Ahmad, A. (2014). Assessment of photogrammetric mapping accuracy based on variation flying altitude using unmanned aerial vehicle. In *IOP conference series: earth and environmental science* (Vol. 18, No. 1, p. 012027). IOP Publishing.

Uysal, M., Toprak, A. S., & Polat, N. (2015). DEM generation with UAV Photogrammetry and accuracy analysis in Sahitler hill. *Measurement*, *73*, 539-543.

Westoby, M. J., Brasington, J., Glasser, N. F., Hambrey, M. J., & Reynolds, J. M. (2012). 'Structure-from-Motion'photogrammetry: A low-cost, effective tool for geoscience applications. *Geomorphology*, *179*, 300-314.

Yilmaz, H. M. (2010). Close range photogrammetry in volume computing. *Experimental Techniques*, *34*(1), 48-54.

Yilmaz, O., & Karakus, F. (2016). Stereo and KinectFusion for continuous 3D reconstruction and visual odometry. *Turk J Eng & Comp Sci, 24*, 2756-5770.

Yoo, I. S. (2015). Disaster planning in Korea. *Hanyang Medical Reviews*, *35*(3), 157-173.

Yoo, Y. H., Choi, J. W., Choi, S. K., & Jung, S. H. (2016). Quality evaluation of orthoimage and DSM based on fixed-wing UAV corresponding to overlap and GCPs. *Journal of the Korean Society for*

Geospatial Information Science, *24*(3), 3-9.

Yu, J. J., Park, H. S., Kim, D. W., Yoon, J. H., & Son, S. W. (2018). Assessing the Applicability of Sea Cliff Monitoring Using Multi-Camera and SfM Method. *Journal of the Korean geomorphological association, 25*(1), 67-80.

Yu, J. J., Son, S. W., Park, H. S., Jeon, H. J., & Yoon, J. H. (2017). Evaluation of DSM Accuracy Based on UAS with Respect to Camera Calibration Methods and Application of Interior Orientation Parameters. *KOREAN JOURNAL OF REMOTE SENSING*, *33*(5), 787-798.

環境省大臣官房廃棄物･リサイクル対策部. (2014). *災害廃棄物対策指針*.

국문 초록

대형 폐기물량 산정을 위한 UAS 와 TLS 기반 공간정보 구축기법 연구

손 승 우

서울대학교 대학원 협동과정 조경학

지도교수: 이 동 근

대형재난 발생에 대한 사전예방부터 대응단계까지 전과정의 체계적이고 효율적인 대처를 통해 인명, 재산, 환경 등의 피해를 최소화하여야 한다. 본 연구는 대형재난 발생 시 대응 과정 중 폐기물량 산정에 집중하여 연구를 수행하였다. 대형폐기물량 산정에 대한 연구는 과거부터 수행되고 있지만 실질적인 측정이 어렵기 때문에 발생 이전의 정보를 이용하여 모델링, 원격탐사 등의 기술을 이용하여 폐기물량을 예측하는 연구가 다수 수행되고 있다. 본 연구에서는 최근 활발하게 이용되고 있는 UAS (Unmanned Aerial

System)를 기반으로 폐기물량을 산정하고 정확도를 평가하며 기존 기술과의 비교와 분석을 수행하고자 하였다.

UAS는 UAV (Unmanned Aerial Vehicle)를 이용하여 영상을 취득하고 분석하는 전반적인 과정이라고 볼 수 있다. UAS를 이용하여 3차원 공간정보를 구축하고 정확도를 평가하는 연구가 과거부터 주로 수행되고 있으며 다양한 분야에 적용되고 있다. 이와 유사하게 TLS (Terrestrial Laser Scanning)를 이용하여 3차원 공간정보를 구축할 수 있는데 측량 분야에서 주로 이용되고 있으며 그 정확성 또한 우수하여 식생, 건축, 토목, 문화재, 지형측량 등 다양한 분야에서 널리 이용되고 있다. 대형폐기물량 또한 TLS를 이용하여 3차원 공간정보 구축 후 산정할 수 있지만 비용, 시간 등의 제약사항으로 인해 활용이 불가능하다고 볼 수 있다.

본 연구는 크게 3가지 부분으로 구분할 수 있다. 첫 번째는

UAS를 이용한 3차원 공간정보 구축과 폐기물량 산정 가능성 모색이다. UAS를 이용하여 3차원 공간정보 구축까지의 과정을 정밀 분석하여 최적의 비행변수와 기타 변수를 도출하여 폐기물량 산정의 가능성을 보고자 하였다. 두 번째는 TLS 기술과 UAS 기술 기반의 3차원 공간정보의 비교와 분석이다. 각각의 3차원 공간정보를 M3C2알고리즘을 이용하여 비교하고 분석하여 최적의 폐기물량 산정 기법을 도출하고자 하였다. 마지막으로 세 번째는 3차원 공간정보의 융합과 효율성 분석이다. 두 가지 기술을 융합하여 3차원 공간정보를 구축하고 효율성을 분석하여 UAS, TLS, 융합기법 세가지 방법론간의 차이와 최적의 폐기물량 산정 기법을 도출하고자 하였다.

주요 비행변수는 비행고도와 영상의 중복도이며 이외 변수는 지상기준점 개수이다. 이 외에도 카메라 내부표정, 짐벌의 흔들림 정

도를 분석하였다. 본 연구를 통해 56개의 케이스 중 최적의 변수를 도출하였으며 과거 연구와는 다르게 고도차이가 많이 나는 폐기물 지역에서는 DW (Distance covered on the ground by on image in Width direction)에 의해 결과가 도출되었다. 일반적으로 고도가 낮을수록 높은 정확도를 가지는 3차원 공간정보를 구축하지만 본 연구에서는 고도가 낮을수록 정확도가 낮아지는 것을 확인하였다.

56개의 케이스 모두 정확도 분석을 실시하였으며 정확도와 폐기물량간의 상관성이 있음을 도출하였다. 3차원 공간정보의 정확도가 높을수록 산정한 폐기물량이 유사했으며 이와 반대로 정확도가 낮은 3차원 공간정보들에서는 폐기물량이 제각각으로 나타나는 것을 확인할 수 있었다. 이러한 일련의 과정을 통해 폐기물량 산정을 위한 UAS 최적 변수를 도출하였으며 3차원 공간정보 기반의 폐기물량 산정 가능성을 확인할 수 있었다.

M3C2알고리즘을 이용하여 UAS와 TLS 기반의 3차원 공간정보를 비교하였으며 이를 통해, 각각의 공간정보가 가지고 있는 장단점을 확인할 수 있었다. 정확도의 경우, UAS기반 3차원 공간정보의 RMSE는 0.032m, TLS의 RMSE는 0.202m로 UAS의 정확도가 더 높은 것으로 나타났다. 두 가지 기술을 융합한 3차원 공간정보의 RMSE는 0.030m로써 세 가지 방법론 중에서 가장 높은 정확도를 보였다. 하지만 효율성 관점에서 분석한 결과, UAS 기반의 3차원 공간정보가 단시간에 높은 정확도를 보이는 결과로 도출됨으로써 대형폐기물량 산정에 최적화된 기술과 방법론을 가지고 있는 것으로 확인할 수 있었다. 이 외에도 비용을 분석한 결과, UAS 기반의 3차원 모형 구축까지 소비된 비용이 TLS에 비해 적은 비용이 소비된 것을 확인할 수 있었다.

대형재난 시 비교적 단시간에 대응하여 피해를 최소화 하고 다

양한 의사결정을 진행해야 하는데, 본 연구를 통해 도출한 UAS 기반의 3차원 공간정보 구축 기법은 대형 폐기물량산정과 공간적 의사결정에 활용할 수 있을 기대한다.

주요어: 3 차원 공간정보, M3C2, 비행변수, 폐기물량 산정

학번: 2014-30797